RICE UNIVERSITY

Engineering protein dependence into ferredoxin-based electron transfer systems

By

Albert Tran Truong

A THESIS SUBMITTED
IN PARTIAL FULFILLMENT OF THE
REQUIREMENTS FOR THE DEGREE

Master of Science

APPROVED, THESIS COMMITTEE

Jonathan Silberg
Jonathan Silberg (Sep 3, 2020 16:27 CDT)

Joff Silberg
Professor, Department of BioSciences

Daniel Wagner
Daniel Wagner (Sep 2, 2020 19:56 CDT)

Daniel Wagner
Professor, Department of BioSciences

George Bennett
George Bennett (Sep 8, 2020 15:44 CDT)

George Bennett
Professor, Department of BioSciences

Caroline Ajo-Franklin
Caroline Ajo-Franklin (Sep 2, 2020 20:26 CDT)

Caroline Ajo-Franklin
Professor, Department of BioSciences

HOUSTON, TEXAS

August 2020

ABSTRACT

Engineering protein dependence into ferredoxin-based electron transfer systems

By

Albert Truong

Electron flow is central to bioenergetics and life, but our ability to control this biological process remains limited. One method of controlling electron flow involves engineering protein electron carriers (PECs) into switches with electron transfer activity that can be actuated under specific conditions. Previous work has created ferredoxins (low-potential PECs) whose activity depends on the presence of specific small molecules by splitting a ferredoxin and fusing the resulting fragments to a pair of proteins that dimerize in the presence of a small molecule or to the termini of a ligand binding domain. These approaches are limited to the specific molecules that can bind these domains to toggle ferredoxin activity. To expand the molecular repertoire for controlling electron transfer, I propose two strategies for constructing ferredoxins whose activity depends on an arbitrary molecule. The first strategy involves fusing a pair of nanobodies which share the same binding target to a pair of split ferredoxin fragments. The presence of the binding target is expected to cause both nanobodies to come together, allowing the ferredoxin fragments to complement and resume ferredoxin activity. To explore this strategy, three different anti-GFP nanobodies were fused in a variety of configurations to a ferredoxin fragment, and GFP was fused to the complementary ferredoxin fragment. Ferredoxin activity was observed when specific configurations of nanobody-ferredoxin and GFP-ferredoxin fusions were co-expressed, indicating the binding of an anti-GFP nanobody to its target can restore ferredoxin activity. However, when two different anti-GFP nanobodies were fused to a pair of split ferredoxin

fragments, the presence of free GFP was unable to toggle ferredoxin activity. The second strategy involves inserting a marginally stable nanobody domain into a ferredoxin, which is unfolded and disrupts ferredoxin activity in the absence of its target protein, but is folded and restores ferredoxin activity in the presence of its target protein. To explore this strategy, three different stable anti-GFP nanobodies were inserted into a ferredoxin, and two of the three were found not to disrupt ferredoxin activity, indicating that these variants are potential targets for laboratory evolution for the desired switch behavior. Successful engineering of chemical-dependent ferredoxin switches may lead to the creation of cellular sensors with electrical output that can interface with electronic devices.

Acknowledgements

I would first like to thank my advisor, Dr. Joff Silberg for his mentorship and support. He has modeled scientific thought and creativity and has motivated me to become a better thinker and scientist.

I want to thank my committee, Dr. George Bennett, Dr. Caroline Ajo-Franklin, and Dr. Daniel Wagner for their feedback on this thesis. I want to also thank the BA-MA-PhD program coordinators Dr. Kathy Matthews, Dr. Michael Stern, Dr. Daniel Wagner, and Dr. Joff Silberg for providing the opportunity to participate in the BA-MA-PhD program. I also want to thank my previous committee, Dr. Natasha Kirienko, Dr. Kathy Matthews, and Dr. Daniel Wagner, for providing guidance during the early stages of my research.

I would like to thank all the past and present members of the Silberg lab, especially my mentors when I was just beginning to do biology research, Dr. Emily Thomas and Barbara Nassif, for their friendship and advice.

Finally, I would like to thank my father and mother, Hao Truong and Hoa Tran, to whom I owe everything, as well as my sisters, Jaycie Truong and Tammy Truong for their friendship and support.

TABLE OF CONTENTS

LIST OF FIGURES

LIST OF TABLES

ABBREVIATIONS

4-HT: 4-hydroxy tamoxifen

AHL: 3-oxo-C12 acyl homoserine lactone

aTc: anhydrotetracycline

Chl^R: chloramphenicol resistance markerKan^R: kanamycin resistance marker

EET: extracellular electron transfer

ET: electron transfer

Fd: ferredoxin

FKBP: FK506 binding protein

Fld: Flavodoxin

FNR: ferredoxin:NADPH reductase

FRB: FKBP rapamycin binding protein

IPTG: Isopropyl β-D-1-thiogalactopyranoside

M9c: modified m9 minimal media with cysteine and methionine

M9sa: modified m9 minimal media without cysteine and methionine

MFC: microbial fuel cell

MHT: methyl halide transferase

PEC: protein electron carrier

PCR: polymerase chain reaction

P_{lac}: IPTG-inducible promoter

P_{lasR}: 3-oxo-C12 AHL-inducible promoter

P_{tet}: aTc-inducible promoter

SIR: sulfite reductase

$Strep^R$: streptomycin resistance marker

Chapter 1: Introduction

1.1 Electron flow is critical to metabolism

Electron flow is an essential component of many metabolic pathways necessary for life. For example, glycolysis is an ancient and ubiquitous energy-obtaining pathway which transfers electrons from glucose to NAD^+ to form NADH, a chemical mediator that is used to drive reduction reactions in the cell (Nelson and Cox, 2017). Another important cellular process is oxidative phosphorylation, which transfers electrons from NADH and $FADH_2$ to the electron acceptor O_2 through an electron transfer (ET) chain, generating a proton gradient needed for ATP generation in the process (Nelson and Cox, 2017). In plants, cyanobacteria, and algae, photosynthesis uses light to oxidize water and obtain an excited electron, which, in a process similar to oxidative phosphorylation, is transferred to various protein and chemical intermediates, producing a proton gradient for ATP generation, before finally reducing $NADP^+$ to NADPH. The ATP and NADPH that is produced is then used to reduce CO_2 to glucose (Nelson and Cox, 2017). These pathways represent only a small fraction of the biological processes which depend on electron flow. In fact, electron flow is essential to all energy metabolism, as all energy in cells is obtained by capturing the energy liberated by the oxidation of molecules.

With glycolysis, oxidative phosphorylation, photosynthesis, and carbon fixation, electrons are transferred to intermediates before reaching their final acceptor. These intermediates, also known as electron carriers, can be small molecules (like NADH, $FADH_2$, and NADPH) or proteins (like ferredoxins, flavodoxins, and cytochromes). Cells regulate electron flow by regulating electron carriers, and protein electron carriers (PECs) can be regulated in ways that are distinct from the small molecule electron carriers. With PECs, electron flow to and from specific donors

and acceptors can be regulated by varying the expression of the PECs (or their partners) using transcription, translation, and post-translational modifications (Kochanowski et al, 2015). Additionally, the physicochemical properties of the PEC, such as midpoint redox potential, number of active sites, partner specificity, and stability and turnover, can be tuned by evolution through mutations in the underlying protein sequence (Battistuzzi et al, 2000, Reeve et al, 1989, Yacoby et al, 2011).

1.2 Our current understanding of electron flow is limited

While metabolic models that describe the carbon flux of *E. coli* have been built and include information about electron flow to some extent by describing the redox reactions involved in metabolite production, no electron flux models exist that detail all the interactions of cellular electron carriers, and protein electron carrier partner specificity has only been mapped in a small number of model organisms (Monk et al 2017). It is possible to identify specific redox reactions that require chemical cofactors like NADPH and NADH using bioinformatics. By querying genomes with protein sequences known to bind these chemicals, additional oxidoreductases possessing cofactor-binding sequences can be found. However, this approach is challenging to apply to determine the binding partners and role of protein electron carriers because some proteins have evolved divergent sequences that make it challenging to anticipate the electron donor or acceptor of oxidoreductases, preventing us from fully understanding how electrons flow through cells.

Though protein electron carriers are not fully understood, bioinformatic studies show that they are present in many different species in many domains of life. A bioinformatic study analyzing the evolution and abundance of low potential ferredoxins (Fd) and flavodoxins (Fld) in different species has found that they are present in many phyla across all domains and that many

organism genomes contain multiple different ferredoxins and flavodoxins (Campbell et al 2019). Out of all the domains, Archaea possess the largest number of ferredoxins and flavodoxins per genome, with a mean of 12.7 PEC genes per organism, while Eukaryotes have the lowest, with a mean of 2.8 PEC genes per organism (Campbell et al 2019). The reason some organisms have such a high abundance of protein electron carrier paralogs is unclear, and the binding partners of these protein electron carriers is also frequently unknown. In the case of ferredoxins, we know how to identify their potential partner proteins by their sequence, but we do not yet know how to predict which specific ferredoxin sequence(s) in a genome act as the electron carrier (Atkinson et al, 2016, Campbell et al 2019). A better understanding of protein electron carriers will improve our understanding of electron flux and metabolism and consequently improve our ability to control electron flux.

1.3 New technologies can be created by rewiring electron flow

Since electron flow is fundamental to cellular function, exerting artificial control over cellular electron flow would allow the development of novel and useful organisms. In metabolic engineering, which focuses on manipulating cellular carbon flux to produce valuable materials, redox imbalances often arise while engineering carbon flux. These shifts in the ratio of the oxidized to reduced form of electron carriers (*e.g.* $NAD(P)^+$/NAD(P)H) to values can result in inefficient chemical production, oxidative stress, or cell death, especially under anaerobic fermentative conditions (Shen et al, 2011). Greater control over electron flow would allow the rational design of synthetic pathways that avoid redox imbalances in cells, helping to improve chemical production efficiency (Wang et al, 2017).

Increased control over cellular electron flow is also necessary to advance bioelectronics, a field that aims to integrate biology and electronics for useful applications. One field of

bioelectronics is microbial electrosynthesis, which uses an applied current to supply electrons to microbes to produce high value chemicals (Lovley, 2011, Nevin et al, 2011). While microbial electrosynthesis offers an alternative way to produce organic products that does not rely on fossil fuels, it has several shortcomings. It is difficult to selectively produce specific products, limiting the efficiency of product synthesis as electrons are diverted to unwanted byproducts. Additionally, the maximum rate of electrons that can be supplied to cells is low, further limiting the production rate of desired products (Prévoteau et al, 2019). More precise control over electron flow may be used to eliminate competing pathways that produce unwanted byproducts and increase the efficiency of electrosynthesis, to avoid redox imbalances, and to increase the rate of electron transfer into cells.

Control over electron flow may also be useful to improve electricity generation with microbial fuel cells (MFCs). In a microbial fuel cell, microbes at the anode of an electrochemical cell oxidize organic metabolites, generating electrons which are then transferred to the anode and flow to the cathode (Logan et al, 2006). One limiting step in electricity generation is transferring electrons liberated by microbial metabolism to the fuel cell anode, as the membranes of microbes are typically electrically insulating (Kim et al, 2007). In engineered systems, electrochemical mediators, which are frequently phenolic compounds that are toxic to cells, are often added to MFC reactors to increase electron transfer rates from microbe to anode (Kim et al, 2007, Jang et al, 2004). While in nature, dissimilatory metal reducing bacteria like *Shewanella oneidensis* and *Geobacter sulfurreducens* have evolved proteinaceous appendages that are capable of extracellular electron transfer (EET) to anodes without mediators (Shi et al, 2016). Improving control of electron flow may allow us to engineer other species not capable of EET to use less toxic mediators

or perform efficient mediator-less extracellular electron transfer (Logan, 2009, TerAvest et al, 2014).

Finally, strategies to couple cellular electron flow to electronic devices could be used to couple cellular sensing to a faster read out than more traditional methods such as the production of light or chemicals. While these latter outputs require light- or chemical-sensing equipment to be read, an electrical output from cells would avoid this need and allow for simplification and miniaturization of biosensing devices like bioelectronic pills (Mimee et al, 2018, Webster et al, 2014).

1.4 Modifying protein electron carriers changes cellular electron flow

Cellular electron flux can be altered through the introduction of new PECs into a cell's genome. In natural systems, cyanophages leverage this approach by introducing phage-encoded PECs in their host after infection, allowing them to redirect electron flow to increase photosynthesis rate, pigment production, and NADPH/$NADP^+$ ratio to increase phage-infected host fitness (Dammeyer et al, 2008, Thompson et al, 2011). While this approach is relatively easy to employ, unless the non-native PEC introduced is well characterized, it is difficult to predict how host electron flow will change in response to non-native PEC expression. We currently cannot predict the effect of introducing non-native PECs on the electron fluxome, since we cannot anticipate a priori how PECs couple with different partner oxidoreductases.

PECs are ideal targets for engineering increased control of electron flow because the genes that encode them can be modified using genetic engineering techniques. Another strategy for controlling electron flow synthetically is to mutate a protein electron carrier in a way that changes its binding partner or cofactor preference. A glucose dehydrogenase, which couples the oxidation of glucose and the reduction of $NAD(P)^+$, has been computationally designed to prefer

nicotinamide mononucleotide (NMN^+), a metabolic precursor to NAD and NADP, over $NAD(P)^+$ (Black et al, 2019). Three substitutions (I195R, A93K, Y39Q) were made to glucose dehydrogenase from *Bacillus subtilis*, which increased its catalytic efficiency toward NMN^+ 1000-fold over wild-type. An additional mutation (S17E) decreased NAD^+ binding, increasing NMN^+ specificity. These modifications allow glucose dehydrogenase to produce a pool of reduced NMN, which can supply reducing power for various biochemical reactions, such as the production of levodione, a pharmaceutical intermediate, without disturbing the native $NAD(P)^+$/NAD(P)H balance. In other work, directed evolution has been used to switch the cofactor preference of a formate dehydrogenase from *Pseudomonas* sp. 101 from NAD^+ to $NADP^+$ (Calzadiaz-Ramirez et al, 2020). A mutant library of formate dehydrogenase was generated and its NADPH regeneration activity was selected for by introducing the library into an *E. coli* NADPH auxotroph. The best formate dehydrogenase variant was 5 times more efficient and 14 times more NADPH-specific than the best previously engineered enzyme. While this approach can achieve specific alterations in electron flow, it is low-throughput and labor intensive, as it requires either computational rational design or the design of an appropriate selection assay.

One final strategy to control electron flow synthetically is to fuse a protein electron carrier to a specific binding partner. In an engineered sorghum system, the native ferredoxin has been fused to cytochrome P450 CYP79A1 and targeted to the chloroplast to redirect electrons that originate from photosystem I towards P450 and its biosynthetic pathways (Mellor et al, 2016). Normally, in the chloroplast, electrons from photosystem I are passed from Fd to ferredoxin NADPH reductase (FNR), but introducing P450 into the thylakoid membrane allows soluble ferredoxin present in the chloroplast to transfer electrons to P450. Introducing a P450-ferredoxin fusion into the thylakoid membrane further increases the specific activity of the P450. Another

fusion, a ferredoxin-hydrogenase fusion has been demonstrated to divert Fd electron transfer away from FNR and towards hydrogenase in isolated thylakoids (Yacoby et al, 2011). While protein fusion can specifically alter electron flow, can promote electron transfer between partners that normally don't interact well, and is less labor intensive than mutation of PECs to alter binding partners, the fusion of one protein to another may unpredictably alter the folding or other properties of the fusion partners, meaning that some desired electron flow alterations may not be possible.

Introducing non-native PECs into cells, mutating PECs to alter binding partners, and fusing PECs to specified binding partners are all approaches that permanently alter electron flux in cells. This means that these strategies are not suitable for applications that require rapid (on the order of seconds), transient modification of electron flux under specific conditions, such as in the construction of cellular sensors with electrical output. A PEC engineered to have ligand-dependent activity would be more useful in such applications.

1.5 Rapid and conditional modification of cellular electron flow has been achieved

PECs switches that display ligand-dependent activity have previously been created. Such switches were built by modifying ferredoxin, an evolutionarily ancient protein electron carriers that carry low-potential electrons (Atkinson et al, 2019). In one such system, the [2Fe-2S] ferredoxin from the thermophilic cyanobacterium *Mastigocladus laminosus* was split and fused to one of a pair of strongly associating leucine zippers. Each fusion was placed under the control of different chemically inducible promoters, allowing for chemical control of electron flow at the level of transcription. Upon induction of transcription and the subsequent translation of the fusions, the ferredoxin fragments complement with the assistance of the leucine zippers, regain function, and allow electron flow (Figure 1.1a). Because transcription and translation must occur before any

electrons are transferred by the ferredoxin, electron transfer lags significantly (30 minutes to several hours) behind the introduction of the inducer molecules. This system is therefore unsuited for applications that require rapid changes in electron flux. To get around this limitation, subsequent switch designs make ferredoxin activity dependent on conditional protein-protein interactions, allowing for fast, post-translational control of electron flow. In one such system, the [2Fe-2S] ferredoxin from *M. laminosus* was split and fused to the rapamycin-inducible dimerizers, FK506 binding protein (FKBP) and FKBP-rapamycin binding domain of mTOR (FRB) (Fish et al, 2005, Woß et al, 2005). Ferredoxin complementation and activity occurred only when the drug rapamycin bound and induced dimerization of FRB and FKBP (Figure 1.1b). Finally, allosteric regulation of ferredoxin activity via 4-hydroxy tamoxifen (4-HT), an estrogen antagonist, was accomplished by inserting the ligand binding domain of the human estrogen receptor into a ferredoxin (Figure 1.1c). In the absence of 4-HT, the ligand binding domain of the estrogen receptor is in a conformation that does not allow for complementation of the ferredoxin fragments fused to its termini. The presence of 4-HT induces a conformational change that brings the ferredoxin fragments close enough to complement and perform electron transfer.

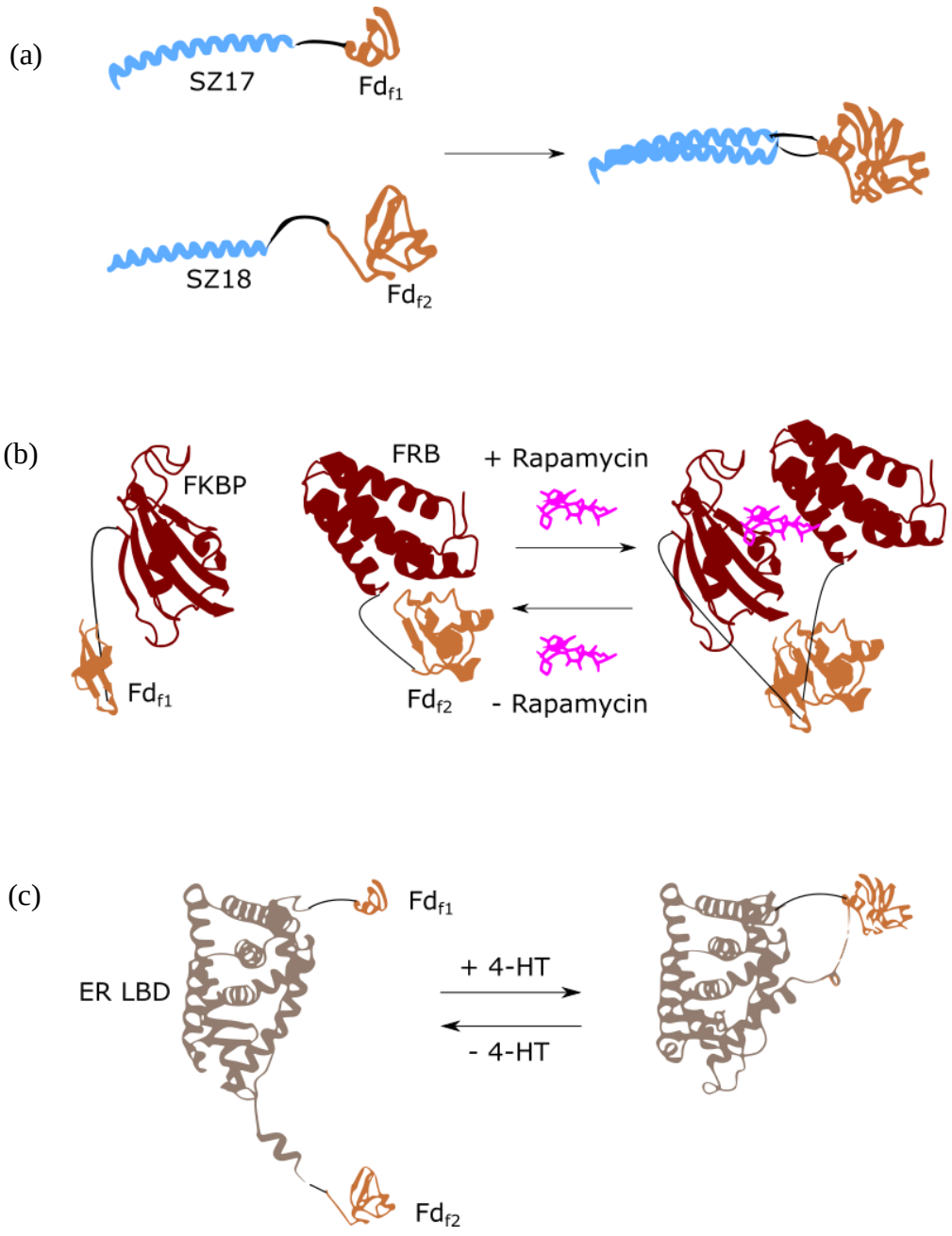

Figure 1.1. Transcriptional and post-translational control of Fd activity. (a) Transcriptional control of electron flow can be achieved by fusing strongly associating leucine zippers to the termini of split ferredoxin fragments. Only when transcription and subsequent expression of both ferredoxin-zipper fusions is induced will electron transfer occur. (b) Post-translational control of electron flow can be achieved by making the complementation of Fd fragments dependent on the presence of a small molecule. In this case, Fd fragments were fused to proteins that only associate when bound to rapamycin. (c) Allosteric control of Fd activity can be achieved by inserting a ligand binding domain into ferredoxin. In this case, inserting an estrogen receptor ligand binding domain that changes conformation when bound to 4-HT causes Fd activity to be dependent on the presence of 4-HT. Adapted from Atkinson et al, 2019.

1.6 Proteins for diversifying post-translational control over electron flow

The post-translational control of ferredoxin activity by fusion to chemically inducible dimerizers or domain insertion is limited because the number of known unique chemically inducible dimerizers or allosterically regulated domains is small. Consequently, only a small number of different chemicals is capable of rapidly toggling ferredoxin electron transfer on and off, limiting the chemical-sensing capabilities of these conditionally active ferredoxins. Additionally, because ferredoxins are cytosolic proteins, extracellular molecules that cannot pass through the porins in a cell membrane or cell wall (which have a ~500 amu size cutoff) cannot be sensed.

To diversify the number of different molecules that control ferredoxin activity, nanobodies, antibody derivatives also known as V_HH antibodies, may be substituted in place of chemically inducible dimerizers or ligand binding domains. Typical antibodies consist of four total proteins—two heavy chains and two light chains—attached to each other by disulfide linkages. Both heavy and light chains contain constant regions, which are identical across different antibodies, and variable regions, which contain the unique protein-binding complementarity determining regions. However, camelids and certain sharks have non-canonical single-domain antibodies which consist only of two heavy chains (Bird et al, 1988). Nanobodies are derived from the variable regions of these camelid and shark single-domain antibodies. They are small (~15 kDa) and require no post-translational modifications to be functional in a variety of cellular systems, which makes them suitable for expression in bacteria. Additionally, the elimination of the antibody constant regions does not affect the ability of nanobodies to bind certain targets. Nanobodies can bind any target capable of being bound by typical antibodies and in fact, due to their small size, can access and bind certain surfaces and molecules that normal

antibodies cannot, including small molecules like testosterone and azo-dyes (Harmsen and DeHaard, 2007, Spinelli, 1996, Spinelli et al, 2001, Li et al, 2016).

Nanobodies against specific antigens can be obtained in several ways. Most commercial services produce nanobodies by immunizing llamas or other camelids against the desired antigen, extracting a library of candidate nanobodies from the blood of the camelid, then screening for suitable nanobodies with various selection techniques such as phage display or yeast display (Pardon et al, 2014). Various synthetic libraries of nanobodies have also been generated which can be screened to select for nanobodies with desired antigen-binding activity (McMahon et al, 2018, Yan et al, 2014).

Two nanobodies that bind to different sites on the same target may be able to act like chemically inducible dimerizers in that the presence of the target will cause the nanobodies to come into proximity with each other, assuming the binding sites are reasonably close (Hill et al, 2018). This property may be exploited to build post-translationally controlled electron flow-mediating systems that can be regulated by almost any molecule or protein that a nanobody can be raised against. The design of this type of regulation would be like the existing post-translational control system, except the chemically inducible dimerizers fused to the ferredoxin fragments would be replaced by nanobodies which share a common target. The presence of the target would cause the two nanobody-ferredoxin fusions to associate, forcing ferredoxin fragment complementation and restoring ferredoxin activity.

An alternative strategy to engineer allosteric control over ferredoxin activity is to insert a conditionally stable nanobody into a ferredoxin. In the absence of the nanobody's target, the nanobody is unfolded and ferredoxin would be unable to perform electron transfer. The binding

of the nanobody to its target stabilizes the nanobody, allowing ferredoxin to perform electron transfer.

1.7 Characterization of protein switches that function in cells

A ferredoxin electron transfer assay has been developed that monitors coupling of a ferredoxin with a pair of donor and acceptor proteins (Atkinson et al, 2019, Wu et al, 2020). This cellular assay was established by creating an *E. coli* strain with a defect in sulfur metabolism, which requires a sulfide-producing pathway dependent on the electron transfer activity of a ferredoxin for growth (Barstow et al, 2011). The pathway is as follows: electrons from NADPH are passed to ferredoxin-$NADP^+$ reductase (FNR) which in turn passes the electrons to ferredoxin. The ferredoxin then supplies the electrons to sulfite reductase (SIR), which requires six electrons to reduce sulfite to sulfide. If ferredoxin is inactive, this electron transfer pathway does not function, sulfide is not produced, and *E. coli* strain is unable to grow in minimal media that contains sulfite as a sulfur source (Figure 1.2). The growth of the sulfide auxotroph is proportional to the amount of ferredoxin-mediated electron transfer that is occurring within the cell and can therefore be used as a reporter of ferredoxin-based protein switch behavior. Thus, this Fd assay is a useful way to study Fd behavior, allowing us an easy way to characterize the activity of Fds in a simple electron transfer pathway. Additionally, because this assay links Fd activity to cell growth, we may also use the assay may to select for Fds with specific properties.

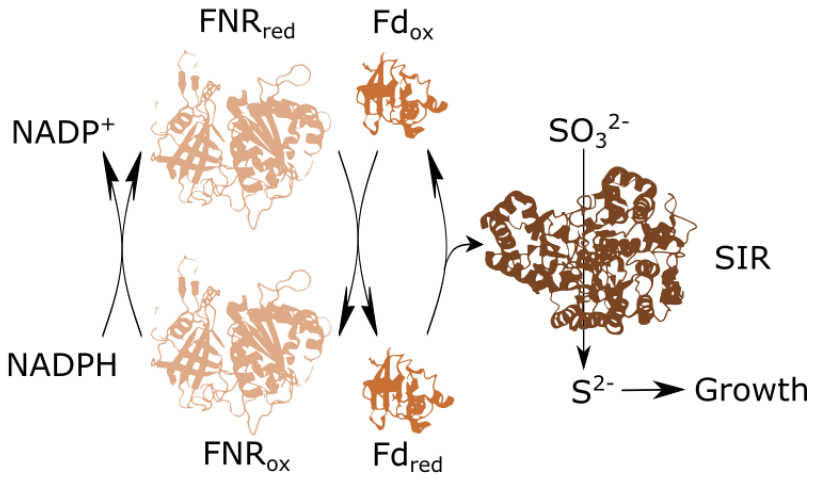

Figure 1.2. The electron transfer activity of ferredoxin can be monitored using a cellular assay. This assay uses growth of a sulfide auxotroph to signal to what extent ferredoxin electron transfer is occurring. An incomplete sulfide-producing pathway is transformed into the sulfide auxotrophic *E. coli* strain EW11. The introduction of a functioning ferredoxin completes this pathway and allows for sulfide production and auxotroph growth to occur.

1.8 Questions addressed in this thesis

Engineering protein-dependent Fd activity through Fd fission and fusion of the resultant fragments to nanobodies raises several questions. First, can the activity of a split Fd be made to depend on the binding of a nanobody to its target? Next, if a specific nanobody-target binding event can control ferredoxin activity, can any nanobody-target pair be used to control ferredoxin activity? If not, then what factors, including fusion linker composition and ferredoxin split site, affect whether ferredoxin activity can be controlled by nanobody-target binding?

Engineering protein-dependent Fd activity through insertion of a conditionally stable nanobody also raises several questions. First, does insertion of an unmodified nanobody into Fd affect Fd electron transfer activity? Also, does nanobody insertion into Fd affect nanobody binding activity? If so, then what factors control whether Fd tolerates nanobody insertion? Finally, can conditionally stable nanobodies be created through random mutagenesis and screening?

Chapter 2: Methods

2.1. Materials

Isopropyl β-D-1-thiogalactopyranoside (IPTG), anhydrotetracycline (aTc), 3-oxo-C12 acyl homoserine lactone (AHL), kanamycin, chloramphenicol, and streptomycin were from Research Product International. E. coli XL1-Blue were from Agilent, Turbo E. coli was from New England Biolabs, and E. coli EW11 was a gift from Pam Silver (Harvard University). All DNA amplification was done through polymerase chain reaction (PCR) using either Phusion or Q5 polymerase. Enzymes for GoldenGate assembly (BsaI and T4 DNA ligase) and Gibson isothermal assembly (T5 exonuclease, Taq ligase, and Phusion polymerase) were from New England Biolabs and Fisher Scientific. Chemicals for growth media were from Fisher Scientific.

2.2. Growth media

All molecular biology was performed using *E. coli* XL1, *E. coli* EW11, or Turbo *E. coli* grown in lysogeny broth (LB). LB medium contained 10 g/L tryptone, 5 g/L yeast extract, 10 g/L NaCl, and enough NaOH to bring the pH of the growth medium to 7. Following transformation with plasmids, *E. coli* was grown in super optimal broth (SOB). SOB medium contained 5 g/L yeast extract, 20 g/L tryptone, 10 mM NaCl, 2 mM KCl, and 20 mM MgSO4, and enough NaOH to bring the pH of the medium to 7.

To condition cells prior to performing selections, *E. coli* EW11 was grown in a modified m9 minimal medium (m9c) that includes both sulfur-containing amino acids. This medium contains sodium phosphate heptahydrate, dibasic (6.8 g/L), potassium phosphate, monobasic (3 g/L), sodium chloride (0.5 g/L), 2% glucose, ammonium chloride (1 g/L), calcium chloride (0.1 mM), magnesium sulfate (2 mM), ferric citrate (500 μM), p-aminobenzoic acid (2 mg/L), inositol

(20 mg/L), adenine (5 mg/L), uracil (20 mg/L), tryptophan (40 mg/L), tyrosine (1.2 mg/L), and the remaining 18 amino acids (80 mg/L each).

To perform selections that depend upon Fd electron transfer, *E. coli* EW11 were grown in a modified m9 minimal medium (m9sa). The medium lacks cysteine or methionine, but is otherwise identical to the m9c medium. *E. coli* EW11 cannot grow in m9sa unless it expresses all three components of a sulfide producing pathway consisting of: ferredoxin NADP reductase (FNR), ferredoxin (Fd), and Fd-dependent sulfite reductase (SIR). Without electron transfer between these proteins, *E. coli* EW11 cannot grow in m9sa (Atkinson et al, 2019, Wu et al 2020).

2.3. Control plasmids

The gene sequences of nanobodies that bind to different DNA epitopes were obtained from a paper by Fridy et al and synthesized by Integrated DNA Technologies, Inc. The nanobodies selected from the paper were originally named LaG-2, LaG-16, and LaG-41 (LaG standing for llama antibody against GFP), but have been renamed Nb2, Nb16, and Nb41. DNA encoding the fluorescent protein mCherry was obtained via amplification from a plasmid gifted by Shyam Bhakta. DNA encoding the pSC101 origin was obtained via amplification from pSH035, a plasmid gifted by Hsiao-Ying (Shelly) Cheng.

Previously described plasmids for complementing EW11 were used as controls and are listed in Table 2.1. These plasmids included: (1) pSAC01 which constitutively expressed corn SIR and corn FNR, (2) pFd007, which uses an aTc-inducible promoter (P_{tet}) to express a ferredoxin from *Mastigocladus laminosus*, and (3) pFd007_C42A, which is identical to pFd007 except for a substitution of alanine for cysteine at residue 42 of the ferredoxin.

Previously described plasmids were also used as the basis for other vectors. These plasmids included: (1) pSH001, which expresses GFP mut3b under control of a 3-oxo-c12 AHL-inducible

promoter, (2) pSH009, which shares the same plasmid backbone as pSH001, but expresses MHT under control of a 3-oxo-c12 AHL-inducible promoter, and (3) pRAP007.35, which expresses two proteins using aTc- and IPTG-inducible promoters. With this last construct, aTc regulates expression of the N-terminal Fd fragment obtained from fission of *Mastigocladus laminosus* Fd after residue 35 fused to FK506 binding protein (FKBP), while IPTG controls the expression of the complementary C-terminal Fd fragment fused to FKBP binding protein (FRB) (fig. 2.1a).

To create a vector that expresses GFP under the control of a 3-oxo-c12-inducible promoter (pSH001_pSC101), the pSC101 origin of replication was cloned into pSH001 in place of the ColE1 origin of replication. To create a similar vector that does not express GFP (pSH009_pSC101), the pSC101 origin of replication was cloned into pSH009 in place of the ColE1 origin of replication.

Table 2.1. Plasmids used as controls and as starting materials for building new plasmids. Plasmids for expressing Fds and GFP were previously described (Atkinson et al, 2019).

Name	**1st gene expressed**	**2nd gene expressed**	**Antibiotic resistance**	**Promoter(s)**	**Origin of replication**
pSAC01	FNR	SIR	$Strep^R$	constitutive	p15a
pFd007	Fd from *M. laminosus*		Chl^R	P_{Tet}	ColE1
pFd007_C42A	Fd C42A		Chl^R	P_{Tet}	ColE1
pSH001	GFP		Kan^R	P_{LasR}	ColE1
pSH009	MHT		Kan^R	P_{LasR}	ColE1
pRAP007.35	Fdf1-FKBP	FRB-Fdf2	Chl^R	P_{Tet} ,P_{Lac}	ColE1
pSH001_pSC101	GFP		Kan^R	P_{LasR}	pSC101
pSH009_pSC101	MHT		Kan^R	P_R	pSC101

2.4 Plasmids for expressing ferredoxins arising from fission after residue 35

Plasmids expressing ferredoxins arising from fission after residue 35 are listed in Table 2.2. To create vectors that express nanobodies as fusions to Fd fragments (p16_2 and p41_2), I cloned nanobody Nb-2 into pRAP007.35 in place of FRB and cloned either nanobody Nb-16 or Nb-41 in place of FKBP (fig. 2.1b).

To create vectors that express nanobodies as fusions to the N-terminal Fd fragment and GFP as a fusion to the C-terminal Fd fragment (p2_GFP, p16_GFP, and p41_GFP), I cloned one of three nanobodies (Nb-2, Nb-16, or Nb-41) into pRAP007.35 in place of FKBP and cloned GFP-mut3b in place of FRB (fig. 2.1c).

To create vectors that express nanobodies as fusions to the C-terminal Fd fragment and GFP as a fusion to the N-terminal Fd fragment (pGFP_2, pGFP_16, and pGFP_41), I cloned one of three nanobodies (Nb-2, Nb-16, or Nb-41) into pRAP007.35 in place of FRB and cloned GFP-mut3b in place of FKBP (fig. 2.1d).

To create vectors that express nanobody-RFP fusions as fusions to Fd fragments, I fused mCherry to nanobody Nb-2 in plasmids p2_GFP and pGFP_2 with a flexible linker (fig 2.1e and f).

Table 2.2. Plasmids expressing fragments from Fd split after residue 35 and fused to other proteins. Flexible linkers with the sequence $(GGGGS)_2AAA$ connect Fd fragments to their fusion mate. Fd fusion 1 is under control of a P_{tet} promoter and Fd fusion 2 is under control of a P_{lac} promoter. Plasmids contain ColE1 origin of replication and chloramphenicol resistance marker.

Name	Fd fusion 1	Fusion 1 linker	Fd fusion 2	Fusion 2 linker
p16_2	Fdf1-Nb16	$AAA(GGGGS)_2$	Nb2-Fdf2	$(GGGGS)_2AAA$
p41_2	Fdf1-Nb41	$AAA(GGGGS)_2$	Nb2-Fdf2	$(GGGGS)_2AAA$
p2_GFP	Fdf1-Nb2,	$AAA(GGGGS)_2$	GFP-Fdf2	$(GGGGS)_2AAA$
pGFP_2	Fdf1-GFP	$AAA(GGGGS)_2$	Nb2-Fdf2	$(GGGGS)_2AAA$
p16_GFP	Fdf1-Nb16,	$AAA(GGGGS)_2$	GFP-Fdf2	$(GGGGS)_2AAA$

pGFP_16	Fdf1-GFP	AAA$(GGGGS)_2$	Nb16-Fdf2	$(GGGGS)_2$AAA
p41_GFP	Fdf1-Nb41	AAA$(GGGGS)_2$	GFP-Fdf2	$(GGGGS)_2$AAA
pGFP_41	Fdf1-GFP	AAA$(GGGGS)_2$	Nb41-Fdf2	$(GGGGS)_2$AAA
p2-RFP_G	Fdf1-Nb2-RFP	AAA$(GGGGS)_2$	GFP-Fdf2	$(GGGGS)_2$AAA
pG_RFP-2	Fdf1-GFP	AAA$(GGGGS)_2$	RFP-Nb2-Fdf2	$(GGGGS)_2$AAA

2.5 Plasmids for expressing ferredoxins arising from fission after residue 55

Plasmids expressing ferredoxins arising from fission after residue 55 are listed in Table 2.3. To create a vector that expresses Fd arising from fission after residue 55, I first created a cloning vector by PCR amplifying a plasmid (pFd007) that encodes a native Fd using primers that create BsaI restriction sites adjacent to the codons encoding residues 55 and 56. In the resulting amplicon, the open reading frames that encode each Fd fragment lie at the opposite ends of the linear DNA. Additionally, DNA sequences encoding *linker-nanobody-*P_{lac}*-gfp-linker* (or *linker-GFP-*P_{lac}*-nanobody-linker*) were PCR amplified from different plasmids (p2_GFP, p16_GFP, p41_GFP, pGFP_2, pGFP_16, and pGFP_41) and cloned into the linear vector. The resulting vectors are identical to their insert donor, except the Fd fragments are the result of Fd fission after residue 55 instead of residue 35.

Table 2.3. Plasmids expressing fragments from Fd split at residue 55 and fused to other proteins. Flexible linkers with the sequence $(GGGGS)_2AAA$ connect Fd fragments to their fusion mate. Fd fusion 1 is under control of a P_{tet} promoter and Fd fusion 2 is under control of a P_{lac} promoter. Plasmids contain ColE1 origin of replication. Plasmids contain ColE1 origin of replication and chloramphenicol resistance marker.

Name	Fd fusion 1	Fusion 1 linker	Fd fusion 2	Fusion 2 linker
p2_GFP.55	Fdf1-Nb2,	$AAA(GGGGS)_2$	GFP-Fdf2	$(GGGGS)_2AAA$
pGFP_2.55	Fdf1-GFP	$AAA(GGGGS)_2$	Nb2-Fdf2	$(GGGGS)_2AAA$
p16_GFP.55	Fdf1-Nb16,	$AAA(GGGGS)_2$	GFP-Fdf2	$(GGGGS)_2AAA$
pGFP_16.55	Fdf1-GFP	$AAA(GGGGS)_2$	Nb16-Fdf2	$(GGGGS)_2AAA$
p41_GFP.55	Fdf1-Nb41	$AAA(GGGGS)_2$	GFP-Fdf2	$(GGGGS)_2AAA$
pGFP_41.55	Fdf1-GFP	$AAA(GGGGS)_2$	Nb41-Fdf2	$(GGGGS)_2AAA$

2.6 Plasmids for expressing split ferredoxin fusions with variable linkers

Plasmids expressing split ferredoxin fusions with variable linkers are listed in Table 2.4. To create a vector expressing Fd fragments fused to other proteins with variable linkers, plasmids p2_GFP and pGFP_2 were modified by shortening or lengthening one or both linkers by one GGGGS repeat.

Table 2.4. Plasmids expressing split Fd fragments fused to other proteins with variable linkers. Fd is split at residue 35. Fd fusion 1 is under control of a P_{tet} promoter and Fd fusion 2 is under control of a P_{lac} promoter. Plasmids contain ColE1 origin of replication and chloramphenicol resistance marker.

Name	Fd fusion 1	Fusion 1 linker	Fd fusion 2	Fusion 2 linker
p2_G_S1	Fdf1-Nb2	AAA(GGGGS)	GFP-Fdf2	$(GGGGS)_2AAA$
p2_G_S2	Fdf1-Nb2	$AAA(GGGGS)_2$	GFP-Fdf2	(GGGGS)AAA
p2_G_S12	Fdf1-Nb2	AAA(GGGGS)	GFP-Fdf2	(GGGGS)AAA
p2_G_L1	Fdf1-Nb2	$AAA(GGGGS)_3$	GFP-Fdf2	$(GGGGS)_2AAA$
p2_G_L2	Fdf1-Nb2	$AAA(GGGGS)_2$	GFP-Fdf2	$(GGGGS)_3AAA$
p2_G_L12	Fdf1-Nb2	$AAA(GGGGS)_3$	GFP-Fdf2	$(GGGGS)_3AAA$
pG_2_S1	Fdf1-GFP	AAA(GGGGS)	Nb2-Fdf2	$(GGGGS)_2AAA$

pG_2_S2	Fdf1-GFP	AAA$(GGGGS)_2$	Nb2-Fdf2	(GGGGS)AAA
pG_2_S12	Fdf1-GFP	AAA(GGGGS)	Nb2-Fdf2	(GGGGS)AAA
pG_2_L1	Fdf1-GFP	AAA$(GGGGS)_3$	Nb2-Fdf2	$(GGGGS)_2$AAA
pG_2_L2	Fdf1-GFP	AAA$(GGGGS)_2$	Nb2-Fdf2	$(GGGGS)_3$AAA
pG_2_L12	Fdf1-GFP	AAA$(GGGGS)_3$	Nb2-Fdf2	$(GGGGS)_3$AAA

2.7 Plasmids for expressing ferredoxins containing an inserted nanobody

Plasmids expressing ferredoxins containing an inserted nanobody are listed in Table 2.5. To create vectors that express Fd containing an inserted nanobody, I excised the portion of the plasmids p2_GFP, p16_GFP, and p41_GFP encoding P_{lac}-*GFP*, then ligated the resulting C terminus of the nanobody to the linker that was formerly fused to GFP.

Table 2.5. Plasmids expressing Fd that has had a nanobody inserted between residues 35 and 36. The nanobody is connected to Fd fragments with flexible linkers with sequence $(GGGGS)_2$AAA. Gene expression is under control of a P_{tet} promoter. Plasmids contain ColE1 origin of replication and chloramphenicol resistance marker.

Name	**Protein expressed**	**Fdf1-Nb linker**	**Nb-Fdf2 linker**
pFd-2-Fd	Fdf1-Nb2-Fdf2	AAA$(GGGGS)_2$	$(GGGGS)_2$AAA
pFd-16-Fd	Fdf1-Nb16-Fdf2	AAA$(GGGGS)_2$	$(GGGGS)_2$AAA
pFd-41-Fd	Fdf1-Nb41-Fdf2	AAA$(GGGGS)_2$	$(GGGGS)_2$AAA

2.8. Cellular assay for monitoring ferredoxin electron transfer

Selections were performed by transforming *E. coli* EW11 with pSAC01, which constitutively expresses the Fd-donor FNR and Fd-acceptor SIR, and plasmids for expressing the

different ferredoxins. Some experiments additionally used cells co-transformed with pSH001, which expresses 3-oxo-C12-inducible GFP. In experiments using two plasmids, streptomycin (100 μg/mL) and chloramphenicol (34 μg/mL) were added to media at all growth steps to maintain plasmids. In experiments using three plasmids, kanamycin (50 μg/mL) was additionally included. Single colonies of *E. coli* EW11 transformed with plasmids were used to inoculate 1 mL m9c cultures. These cultures were grown in deep-well 96-well plates for 18 h at 37 °C while shaking at 250 rpm. An aliquot (1 μL) of the resulting stationary-phase cultures were used to inoculate 1 mL m9sa containing antibiotics using a multichannel pipette. The resulting cultures were then grown in deep-well 96-well plates for 96 hrs at 37 °C while shaking 250 rpm. Every 24 hrs, the optical density (OD) and fluorescence of a 100 μL culture sample was measured.

2.9. Spectroscopy

A TECAN Infinite Pro 200 plate reader or TECAN Spark were used to perform optical density (OD) measurements at 600 nm and fluorescence measurements ($\lambda_{excitation}$ = 488 nm; $\lambda_{emission}$ = 509 nm). Fluorescence was normalized to OD and reported as Fl/OD, where Fl is the fluorescence measurement in arbitrary units.

2.10. Structural analysis

Pymol was used to analyze protein structure and generate protein structure figures. The measurement wizard in Pymol was used to calculate the distance between the alpha carbons of terminal residues.

2.11. Statistics

Data shown are the mean of a minimum of 3 biological replicates obtained by picking separate colonies from an agar plate. Error bars represent standard deviation. Significance of growth complementation was determined by two-sample two-tailed t-tests.

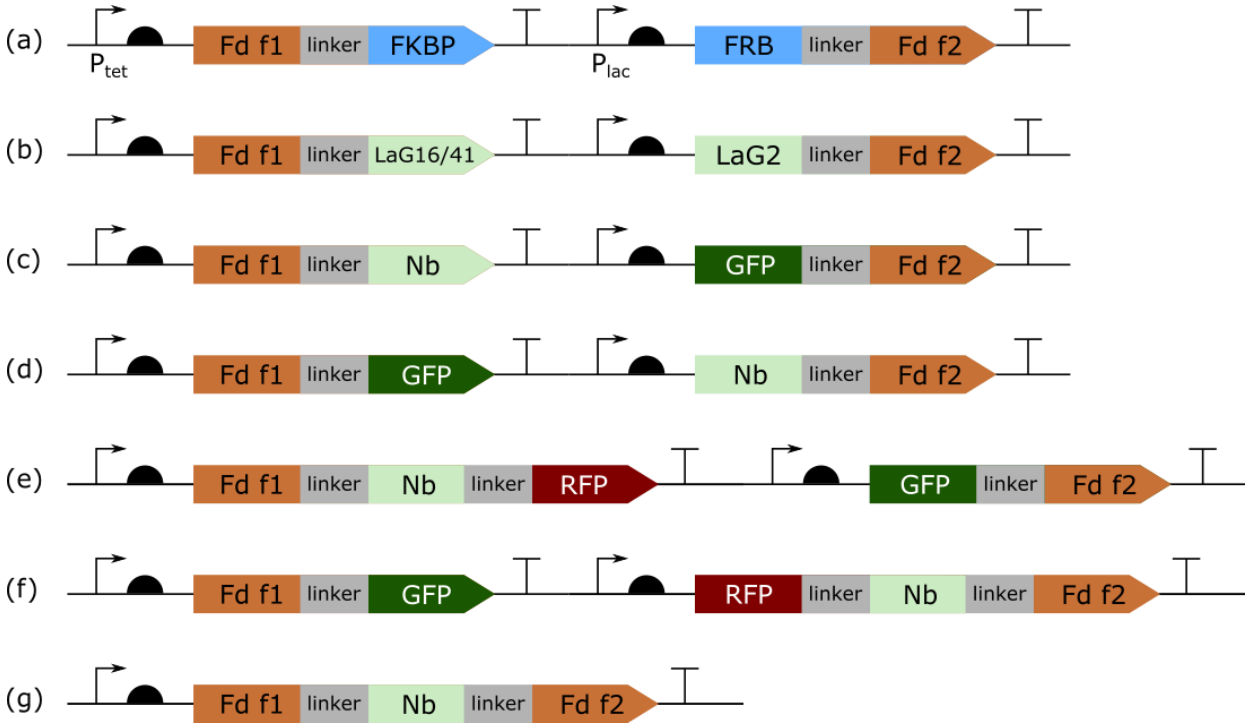

Figure 2.1. Design of constructs used in this thesis.

Chapter 3: Results & Discussion

3.1 Design strategy for antibody-regulated cellular electron transfer

Diverse protein design strategies have been reported that enable the creation of Fd switches whose activity depends on the presence of specific molecules. One strategy involves the splitting of a Fd and using flexible linkers to fuse the resulting fragments to a pair of proteins that dimerize in the presence of a small molecule (also known as chemically inducible dimerizers). In the absence of a specific small molecule, dimerizers cannot associate and the PEC fragments cannot function as electron carriers; in the presence of the molecule, the dimerizers bind the molecule and undergo a conformational change that causes their association. This dimerization event brings the PEC fragments in proximity to one another, aiding ferredoxin complementation and restoring ferredoxin function. However, the number of different molecules that can trigger the protein switch is limited by the repertoire of chemically inducible dimerizers, which is small and contains no large molecule or protein-induced dimerizers. This limits the switch's usefulness in applications like metabolic engineering and biosensing. One way to introduce protein-dependence to this design is to replace the chemically inducible dimerizers with a pair of nanobodies that bind the same protein target. The nanobodies may act like chemically inducible dimerizers in that the presence of the target protein may cause the nanobodies to bind near each other, causing ferredoxin complementation and restoring ferredoxin electron transfer (Figure 3.1).

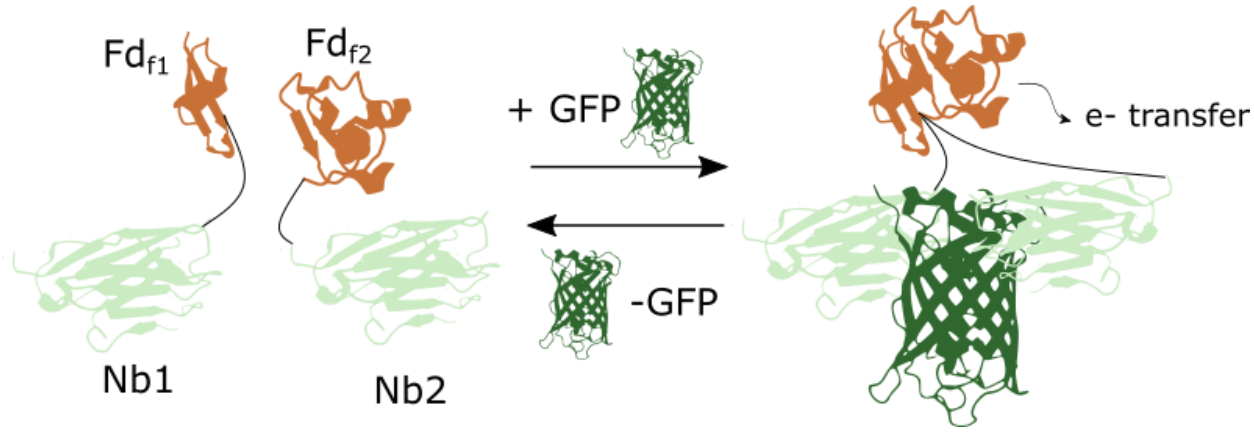

Figure 3.1. Nanobodies can be used to increase the number of molecules that can toggle ferredoxin activity. The number of different molecules that can post-translationally control the flow of electrons in cells can be increased by switching out the chemically induced dimerizers for nanobodies that bind the same arbitrary molecule. The nanobodies act as like chemically induced dimerizers so that the presence of the molecule causes ferredoxin complementation.

Another strategy that has been used to create chemical-dependent Fd switches involves splitting a Fd and using flexible linkers to fuse the resulting fragments to the termini of a ligand binding domain which changes conformation depending on whether or not its ligand is bound. When there is no ligand present, the termini of the ligand binding domain are far apart from one another, separating the ferredoxin fragments and preventing complementation and electron transfer. When ligand is present, a conformational change occurs that brings the ligand binding domain termini closer together, allowing ferredoxin conformation and restoring electron transfer. This design strategy also limits the number of different molecules that can toggle ferredoxin activity because the number of different ligand binding domains that display large chemically induced conformational changes is small. One way to introduce protein dependence into this design involves insertion of a conditionally stable nanobody into a Fd, with flexible linkers separating the nanobody and Fd domains. When the nanobody's target protein is absent, the nanobody is unfolded and the ferredoxin fragments are too far apart to complement well. When the nanobody's target protein is present, the nanobody folds and the ferredoxin fragments are brought close enough to complement and perform electron transfer (Figure 3.2).

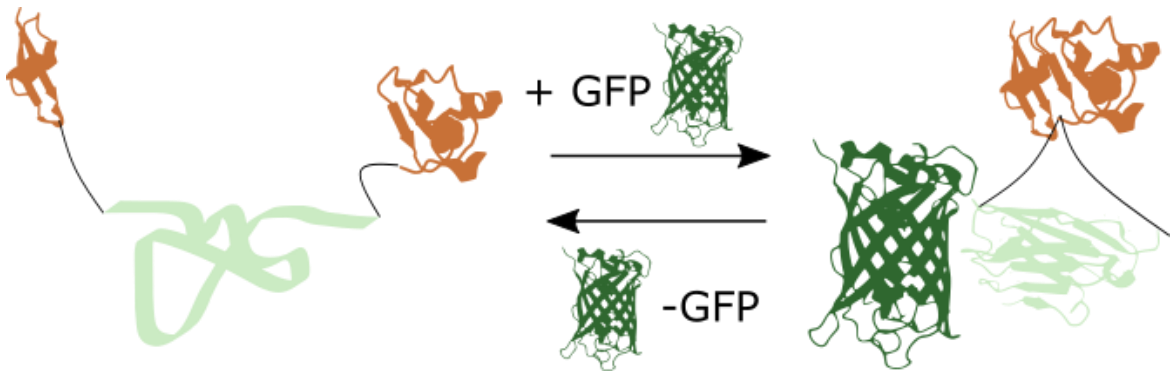

Figure 3.2. Nanobody domain insertion can make Fd activity depend on the presence of a free protein. To create a protein-dependent ferredoxin, a nanobody can be inserted into the ferredoxin, then mutated to be unfolded in the absence of its target protein. When the nanobody is unfolded, the Fd fragments fused to the nanobody termini are unable to complement and perform electron transfer. When the target protein is present, the nanobody is stabilized and the ferredoxin fragments can complement and perform electron transfer.

To create a protein-dependent Fd with these nanobody-based designs, each of the four components (Fd, target protein, linker, and nanobodies) must meet several criteria. The Fd must be tolerant of fission and/or domain insertion; the flexible linkers should allow for the complementation of Fd fragments; the nanobodies must both bind the target protein and tolerate fusion of a Fd fragment to one of their termini; and the target protein should be something whose expression is easy to induce in *E. coli* and to monitor in order to verify whether the engineered Fds are truly dependent on the presence of the target protein. For my specific implementation of these designs, I will use Fd from the thermophilic cyanobacterium *Mastigocladus laminosus* because this particular Fd has already been engineered to display small molecule-dependent activity and has been demonstrated to be tolerant of fission and domain insertion after residue 35 and 55. I will use linkers with the sequence $(GGGGS)_2AAA$ because they too have been used in the design of a small molecule-dependent Fd. I will use GFP as the target protein because it is well-characterized and because its fluorescence makes its expression easily monitored. Finally, I have selected three different anti-GFP nanobodies (named Nb2, Nb16, and Nb41) to use, each a

high affinity binder of a unique site on GFP, from a group of anti-GFP nanobodies generated by Fridy et al (Figure 3.3).

Name	K_d	Binding site
LaG-2	0.7 nM	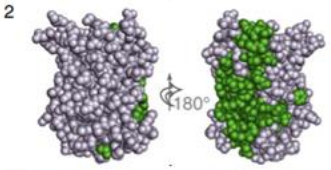
LaG-16	0.9 nM	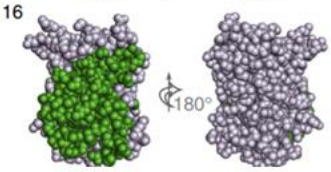
LaG-41	16 nM	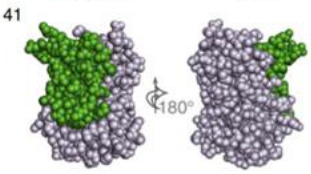

Figure 3.3. Name, dissociation constants and GFP binding sites of selected anti-GFP nanobodies generated by Fridy et al. Highlighted regions (green) denote the sites on GFP at which the nanobodies bind. Adapted from Fridy et al, 2014.

3.2 Nanobody-GFP binding can support split ferredoxin activity

The design involving nanobody fusion to Fd fragments requires that the binding of the nanobodies to their target will cause the Fd fragments to complement and restore electron transfer activity. To test whether this is true, I have cloned a two-hybrid system in which an anti-GFP nanobody and GFP each are fused to the terminus of one of a pair of split ferredoxin fragments (Figure 3.4). Fd from *Mastigocladus laminosus* was split after residue 35, and the resulting Fd fragments, the nanobody, and the GFP were fused in two different arrangements. In the first, the N-terminus of the nanobody was fused to the C-terminus of the first Fd fragment (which contains the original N-terminus of the Fd) and the C-terminus of GFP was fused to the

N-terminus of the second fragment (which contains the original C-terminus of the Fd). In the second, the positions of GFP and nanobody were reversed: the N-terminus of the GFP was fused to the C-terminus of the first ferredoxin fragment, and the C-terminus of the nanobody was fused to the N-terminus of the second fragment. The expression of the two fusions was put under the control of different chemically-inducible promoters, P_{tet} and P_{lac}, which are induced by anhydrotetracycline (aTc) and isopropyl β-D-1-thiogalactopyranoside (IPTG), respectively. All possible combinations of the selected nanobody and two fusion arrangements were successfully cloned to produce a total of six different constructs (Figure 3.5).

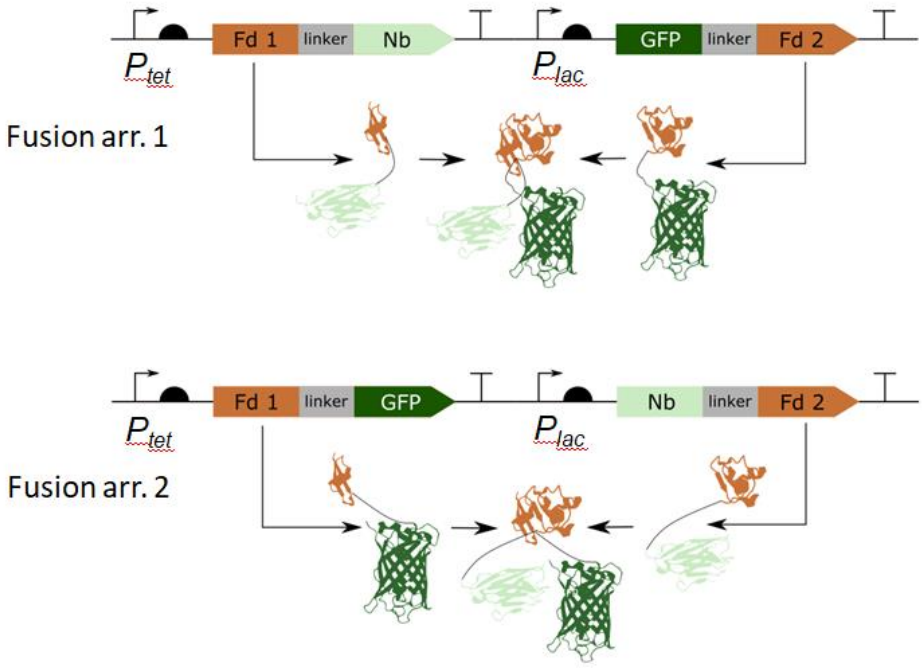

Figure 3.4. A two-hybrid system can assess whether nanobody binding to a protein target is sufficient to cause ferredoxin complementation. This system is built by splitting ferredoxin and fusing a nanobody and GFP to the new termini that are created. Expression of both fragments should lead to ferredoxin complementation and electron flow.

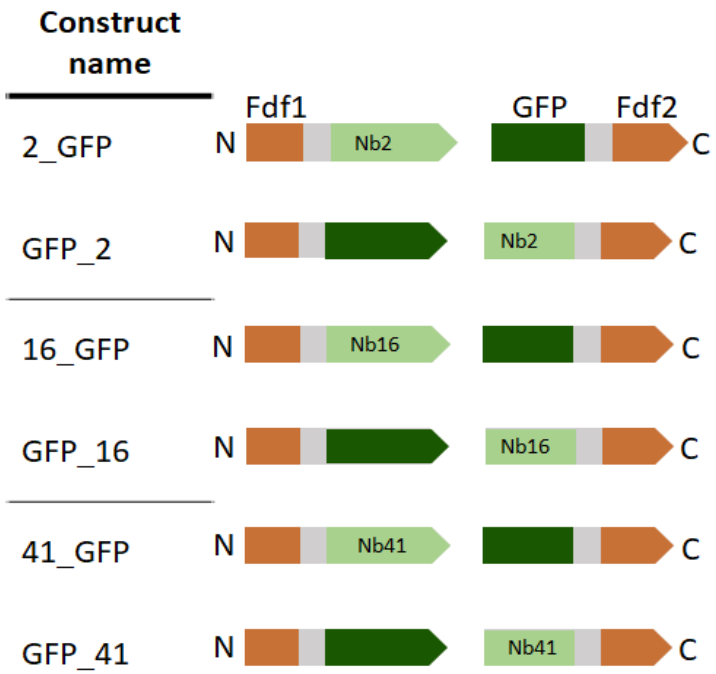

Figure 3.5. Name and design of generated two-hybrid systems. Ferredoxin fragments were split at residue 35 and the resulting termini were fused to nanobody and GFP in two configurations. In one, the C-terminus of the first fragment was fused to the N-terminus of a nanobody and the N-terminus of the second fragment was fused to the C-terminus of GFP. The combination of the two arrangements and three different nanobodies yields six possible two-hybrid systems. The first fusion was put under the control of the P_{tet} promoter, which can be induced by aTc and the second fusion was put under the control of the P_{lac} promoter, which can be induced by IPTG.

If Fd-target binding can cause Fd fragment complementation and restore electron transfer activity, then expression of both fusions encoded in each construct should result in ferredoxin-dependent electron transfer, which can be monitored with a cellular assay that links growth of a sulfide auxotroph to ferredoxin electron transfer. Cell growth indicating ferredoxin activity was seen for four of the two-hybrid systems (named 2_GFP, 16_GFP, GFP_16, and GFP_41) only when expression of both fusions was induced with 100 ng/mL aTc and 100 µM IPTG (Figure 3.6a and b). For the two remaining two-hybrid systems (41_GFP and GFP_2), no growth was seen even when both protein fusions were expressed. To test whether the magnitude of electron transfer depended on the amount of ferredoxin-GFP fusion available in the cell, expression of

ferredoxin-GFP fusion in the construct 16_GFP was varied using different amounts of IPTG while the expression of ferredoxin-nanobody fusion was kept constant. Higher induction of ferredoxin-GFP fusion expression resulted in higher cell growth (Figure 3.6c). Since *M. laminosis* Fd also tolerates fission after residue 55, I also cloned six additional constructs, which differ from the original two-hybrid constructs only in the site of Fd fragmentation, and tested their behavior in the ferredoxin electron transfer assay. The assay results at early time points for each 55 split site construct are similar to their 35 split site counterparts: when expression of both fusions was induced with 100 ng/mL aTc and 100 μM IPTG cell growth was seen for 2_GFP.55, 16_GFP.55, and GFP_41.55 but not for GFP_2.55, GFP_16.55 and GFP_41.55 (Figure 3.7). However, the uninduced negative controls in later time points showed unexpected growth, so these experiments should be repeated (data not shown).

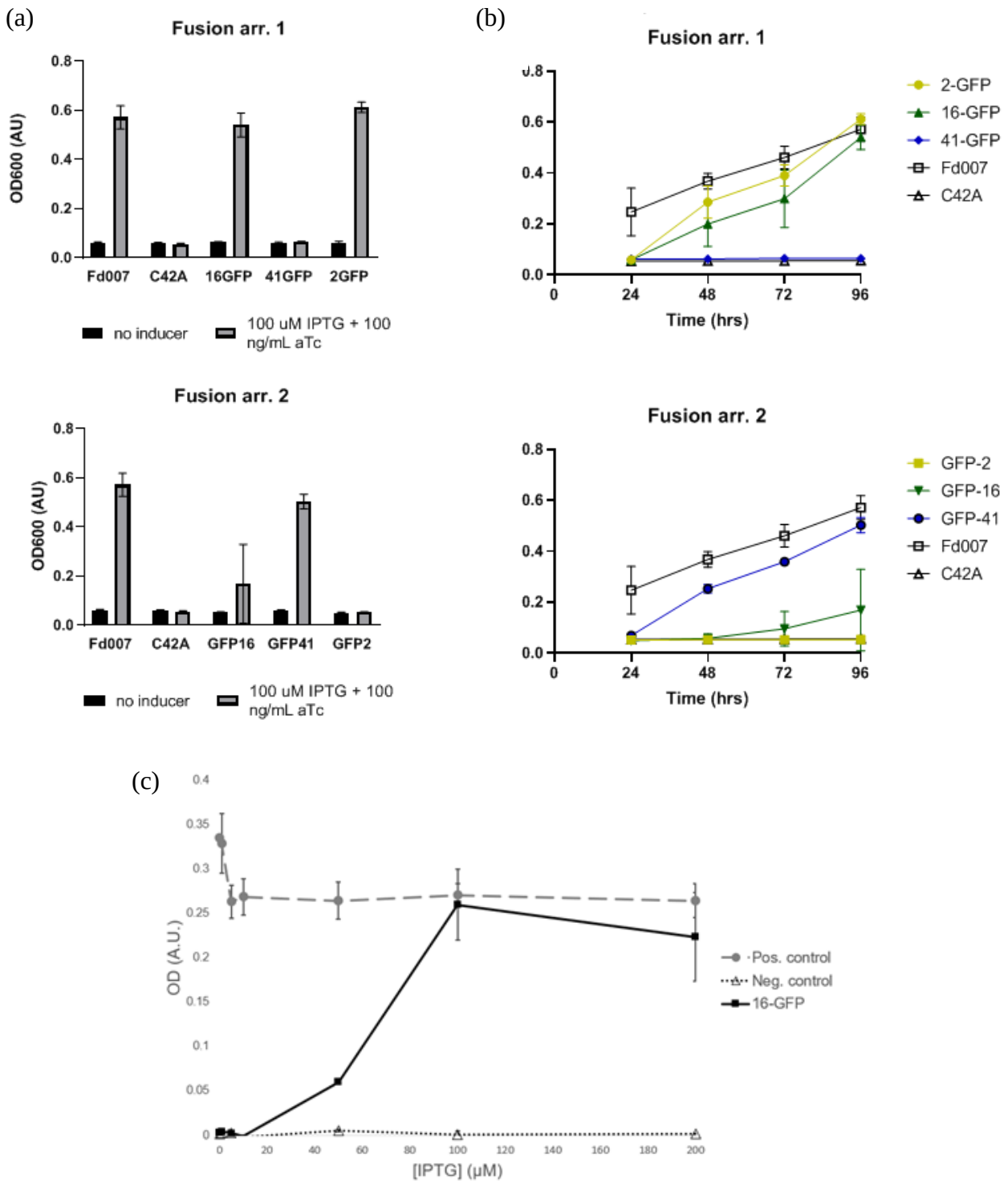

Figure 3.6. Nanobody-GFP binding can restore ferredoxin activity in an induction-dependent manner for two-hybrid systems containing Fd split after residue 35. (a) The ability of the different nanobody-GFP binding interactions to cause ferredoxin complementation in the different two-hybrid systems was assessed using the sulfide auxotroph assay. An unsplit *Mastigocladus laminosus* ferredoxin (Fd007) was used as a positive control and a C42A mutant of the same ferredoxin, which is unable to bind its iron-sulfur cluster, was used as a negative control. The bars display the OD600 of cultures after 96 hours of growth in M9sa minimal media without sulfide. Error bars

represent the standard deviation of three replicates. Four of the six two-hybrid systems (2_GFP, 16_GFP, GFP_16, and GFP_41) show electron transfer activity when expression of both the ferredoxin-nanobody and ferredoxin-GFP fusions were induced with 100 ng/mL aTc and 100 µM IPTG. The two remaining two-hybrid constructs (GFP_2 and 41_GFP) do not show electron transfer activity even when induced. (b) Electron transfer activity of the two-hybrid systems over time. The data points display the OD600 of cultures after 24, 48, 72, and 96 hours of growth in M9sa minimal media without sulfide. Error bars represent the standard deviation of three replicates. (c) The electron transfer activity of the two-hybrid construct 16_GFP is dependent on the level of transcriptional induction of one of the fragments. One fusion was induced with a constant concentration of 100 ng/mL aTc while the other fusion was induced at variable levels using an IPTG titration with concentrations of 0, 1, 5, 10, 50, 100 and 200 μM. The growth of sulfide auxotrophic cells transformed with 16_GFP was assessed after 48 hours of growth in minimal media lacking sulfide. Error bars represent the standard deviation of three replicates. Higher concentrations of IPTG led to greater growth in the assay up to a concentration of 100 μM, after which growth seemed to drop.

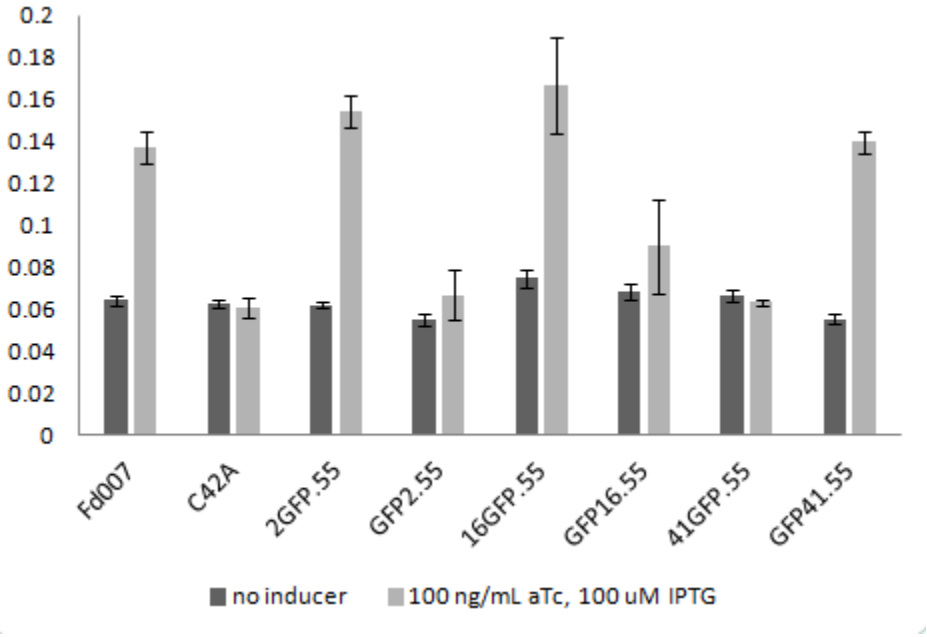

Figure 3.7. Nanobody-GFP binding can restore ferredoxin activity in an induction-dependent manner for two-hybrid systems containing Fd split after residue 55. The ability of the different nanobody-GFP binding interactions to cause ferredoxin complementation in the different two-hybrid systems was assessed using the sulfide auxotroph assay. The bars display the OD600 of cultures after 24 hours of growth in M9sa minimal media without sulfide. Error bars represent the standard deviation of three replicates. Three of the six two-hybrid systems (2_GFP.55, 16_GFP.55, and GFP_41.55) show electron transfer activity when expression of both the ferredoxin-nanobody and ferredoxin-GFP fusions were induced with 100 ng/mL aTc and 100 µM IPTG. The three remaining two-hybrid constructs (GFP_2, GFP16.55, and 41_GFP) do not show electron transfer activity even when induced.

These data are interesting in that switching the positions of the GFP and nanobody of each construct reverses its behavior in the assay. Constructs that show high electron transfer

activity in the assay (2_GFP, 16_GFP, and GFP_41) each have mirrors with alternate fusion arrangements that show poor-to-no electron transfer activity (GFP_2, GFP_16, and 41_GFP). This indicates that the binding of nanobody to GFP can cause ferredoxin complementation, but only for a specific combination of nanobody and fusion arrangement. Since each of the three nanobody variants is a component of at least one construct that shows expected behavior in the assay, it is unlikely that unexpected assay behavior can be attributed to one component of the two-hybrid system in isolation, such as a "dud" nanobody which is intrinsically unable to bind GFP. Rather, it is more likely that some interaction between the two-hybrid system components is responsible for the failure to exhibit electron transfer. It is necessary to explore which specific aspects of the fusion arrangements are responsible for controlling the electron transfer ability of these systems.

3.3 Investigating the effects of linker length

An initial hypothesis that attempted to explain the poor electron transfer activity of certain two-hybrid systems is that the fusion of the ferredoxin to the nanobody causes steric hindrance that physically blocks the nanobody from binding its target. This hypothesis is unlikely: nanobodies have a conserved structure in which the N-terminus faces the nanobody target; therefore, fusion at the N-terminus of the nanobody is most likely to cause steric hindrance. However, the two-hybrid variants 2_GFP and 16_GFP have this arrangement yet still function.

Another hypothesis is that, in poorly functioning two-hybrid systems, the Fd fragments are unable to come close to one another in the nanobody-GFP complex due to the inability of the linkers to bridge the distance between the termini of the nanobody and GFP. This hypothesis is

supported by the structure of a nanobody-GFP complex (Figure 3.8). The distance between the N-terminus of the nanobody and the C-terminus of the GFP is smaller than the distance between the C-terminus of the nanobody and the N-terminus of the GFP. It is expected, then, that the systems in which ferredoxin is fused to the N-terminus of the nanobody and the C-terminus of the GFP are more likely to allow ferredoxin complementation. This is supported by experiments that show that the majority of the systems with this arrangement (2_GFP and 16_GFP but not 41_GFP) show electron transfer activity. To test if linker length affects ferredoxin complementation, I have modified the linkers of the constructs 2_GFP and GFP_2 by shortening or lengthening one or both of linkers by one GGGGS repeat. If the linker length does affect Fd complementation, then it is expected that shortening the linkers of the functional construct (2_GFP) will decrease its electron transfer activity while lengthening the linkers of the non-functional construct (GFP_2) will increase its electron transfer activity.

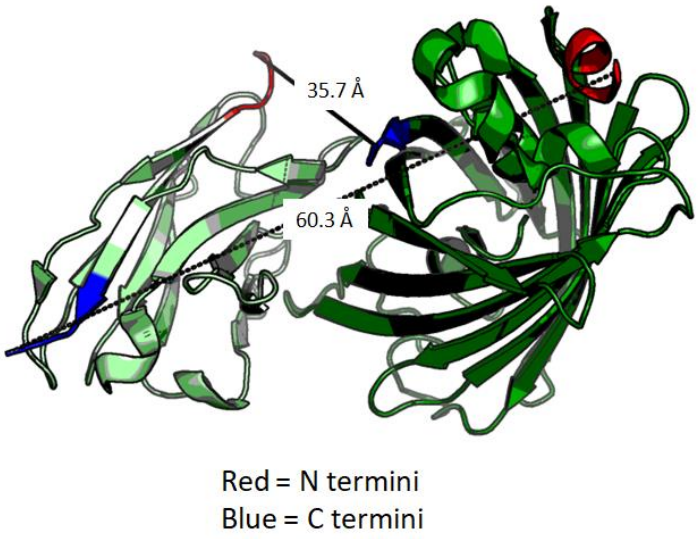

Figure 3.8. Distance between the termini of nanobody and GFP in a binding complex (PDB accession 3OGO). Nanobodies have a conserved structure in which the loops responsible for specific binding to a target protein are near their N-termini (highlighted in red). Consequently, Fd fragments fused to the nanobody N-termini (red) and GFP C-termini (blue) will most likely be closer to each other than Fd fragments fused to the nanobody C terminus (blue) and GFP N-terminus (red) in a nanobody-GFP complex.

Varying the linkers of the construct 2_GFP does not affect its performance in the Fd electron transfer assay. When expression of both fusions was induced with 100 ng/mL aTc and 100 µM IPTG, all altered linker variants of the 2_GFP construct displayed similarly high electron transfer activity, like that of the original construct (Figure 3.9a, b, and c).

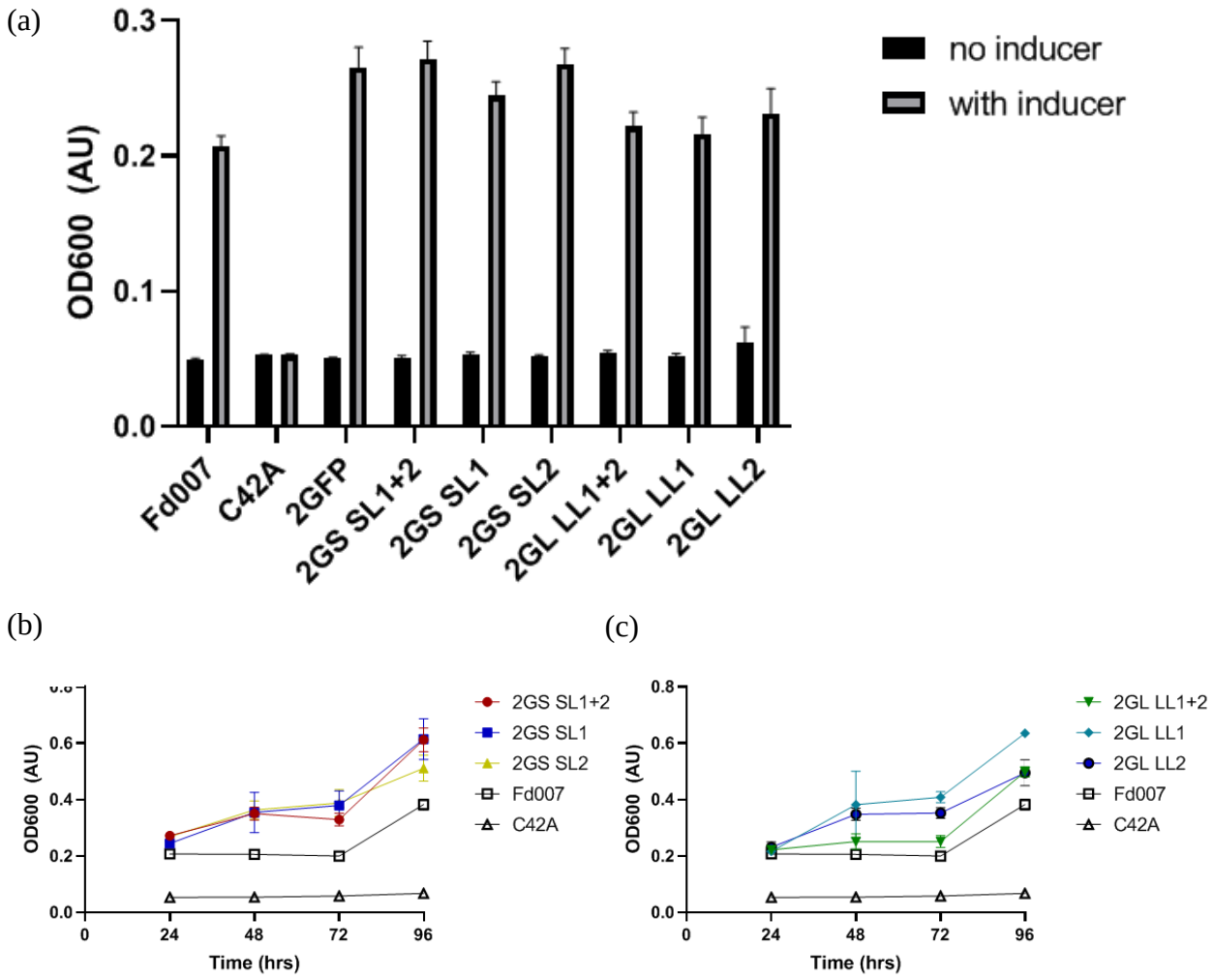

Figure 3.9. Altering the linker lengths of the 2_GFP construct does not abolish its electron transfer activity in a ferredoxin activity assay. (a) One (2GS_SL1 or 2GS_SL2) or both (2GS_SL12) linkers in the 2_GFP construct were shortened by a GGGGS repeat, and one (2GL_LL1 or 2GL_LL2) or both (2GL_LL12) linkers in the 2_GFP construct were lengthened by a GGGGS repeat. The ability of these altered linker constructs to perform electron transfer was assessed using the sulfide auxotroph assay. The bars represent the OD600 of cultures after 24 hours of growth in M9sa minimal media without sulfide. Error bars represent the standard deviation of three replicates. All six altered linker constructs showed electron transfer activity in the assay like that of the original 2_GFP construct

when their expression was induced by 100 ng/mL aTc and 100 µM IPTG. (b) Electron transfer activity of shortened linker constructs over time. One (2GS_SL1 or 2GS_SL2) or both(2GS_SL12) linkers in the 2_GFP construct were lengthened by a GGGGS repeat. The data points represent the OD600 of cultures after 24, 48, 72, and 96 hours of growth in M9sa minimal media without sulfide. Error bars represent the standard deviation of three replicates. All three lengthened linker constructs showed electron transfer activity in the assay like that of the original 2_GFP construct when their expression was induced by 100 ng/mL aTc and 100 µM IPTG. (c) Electron transfer activity of lengthened linker constructs over time. One (2GL_LL1 or 2GL_LL2) or both (2GL_LL12) linkers in the 2_GFP construct were lengthened by a GGGGS repeat. The data points represent the OD600 of cultures after 24, 48, 72, and 96 hours of growth in M9sa minimal media without sulfide. Error bars represent the standard deviation of three replicates. All three lengthened linker constructs showed electron transfer activity in the assay like that of the original 2_GFP construct when their expression was induced by 100 ng/mL aTc and 100 µM IPTG.

Similarly, varying the linkers of the construct GFP_2 does not affect its performance in the Fd electron transfer assay. When expression of both fusions was induced with 100 ng/mL aTc and 100 µM IPTG, all altered linker variants of the GFP_2 construct displayed similarly low electron transfer activity, like that of the original construct (Figure 3.10).

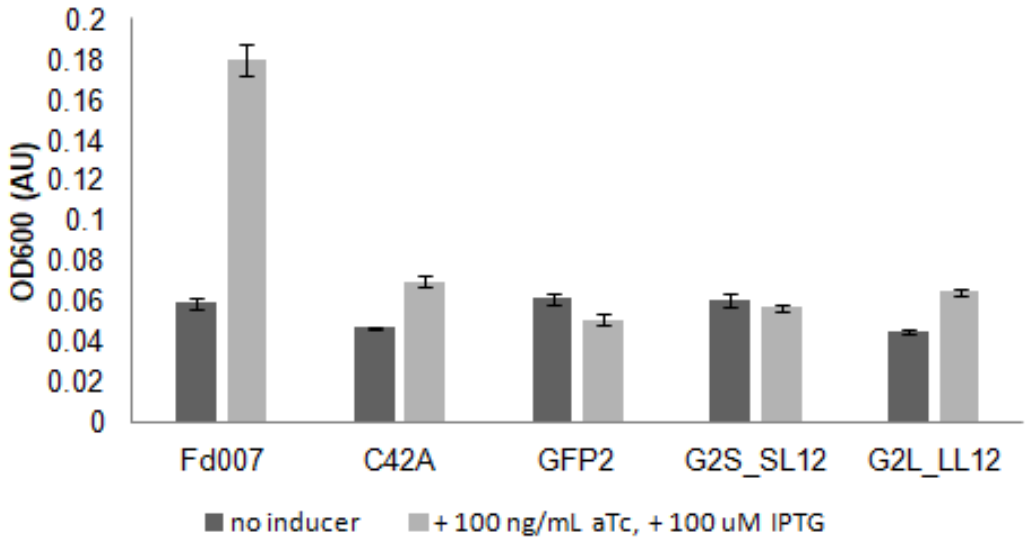

Figure 3.10 Altering the linker lengths of the GFP_2 construct does not alter its inability to perform electron transfer in a ferredoxin activity assay. Both linkers in the GFP_2 construct were shortened (G2S_SL12) by a GGGGS repeat, or lengthened (GSL_LL12) by a GGGGS repeat. The ability of these altered linker constructs to perform electron transfer was assessed using the sulfide auxotroph assay. The bars represent the OD600 of cultures after 24 hours of growth in M9sa minimal media without sulfide. Error bars represent the standard deviation of three replicates. Both altered linker constructs showed no or poor electron transfer activity in the assay like that of the original GFP_2 construct when their expression was induced by 100 ng/mL aTc and 100 µM IPTG.

These data suggest that linker length is not an important determinant of ferredoxin complementation. While these experiments do not rule out the possibility that linker length may affect two-hybrid system electron transfer activity, it is more likely that other factors are primarily responsible for determining the electron transfer activity of the two-hybrid systems. One possibility is that, in the non-functional constructs, the fusion of the particular nanobody and Fd fragment causes the nanobody to be unable to bind GFP due to misfolding or other malfunctions. Future work may test this through a pull-down assay that assesses whether a Fd-nanobody fusion is pulled down with an affinity-tagged GFP.

3.4 Coupling GFP expression to cellular electron transfer

A system that rapidly alters electron transfer activity in response to an arbitrary protein is the goal of this project. One way to accomplish this control of electron flow is to split Fd and fuse nanobodies which bind to the same target to the Fd fragment termini to create a three-hybrid system. This nanobody pair should act similarly to chemically induced dimerizers to form a nanobody-target-nanobody complex when the target molecule is present (Figure 3.1). The nanobody-target-nanobody complex should cause ferredoxin complementation and electron flow. This three-hybrid system is expected to exhibit electron transfer activity only when a target molecule is present and both ferredoxin-nanobody fusions are expressed. As a proof of concept, I have cloned two variants of this design. *M. laminosus* Fd was split after residue 35 and nanobodies were fused to the new termini, and the N-terminus of either Nb16 or Nb41 was fused to the first ferredoxin fragment, and the C-terminus of Nb2 was fused to the second ferredoxin fragment. The fusions were placed under the control of the inducible promoters P_{tet} and P_{lac}. Each nanobody pair in this system was chosen such that the nanobodies bound at different sites

on the GFP. This is to avoid nanobody competing for the same binding site on GFP, which would result in only one ferredoxin-nanobody fusion being able to bind GFP at a time.

The ability of the GFP to control electron flow in the three-hybrid system was tested using the Fd electron transfer assay. When expression of both Fd-nanobody fusions and of GFP was induced with 100 ng/mL aTc, 100 µM IPTG, and 100 nM AHL, respectively, the expected growth did not occur, indicating a failure of ferredoxin to complement (Figure 3.11).

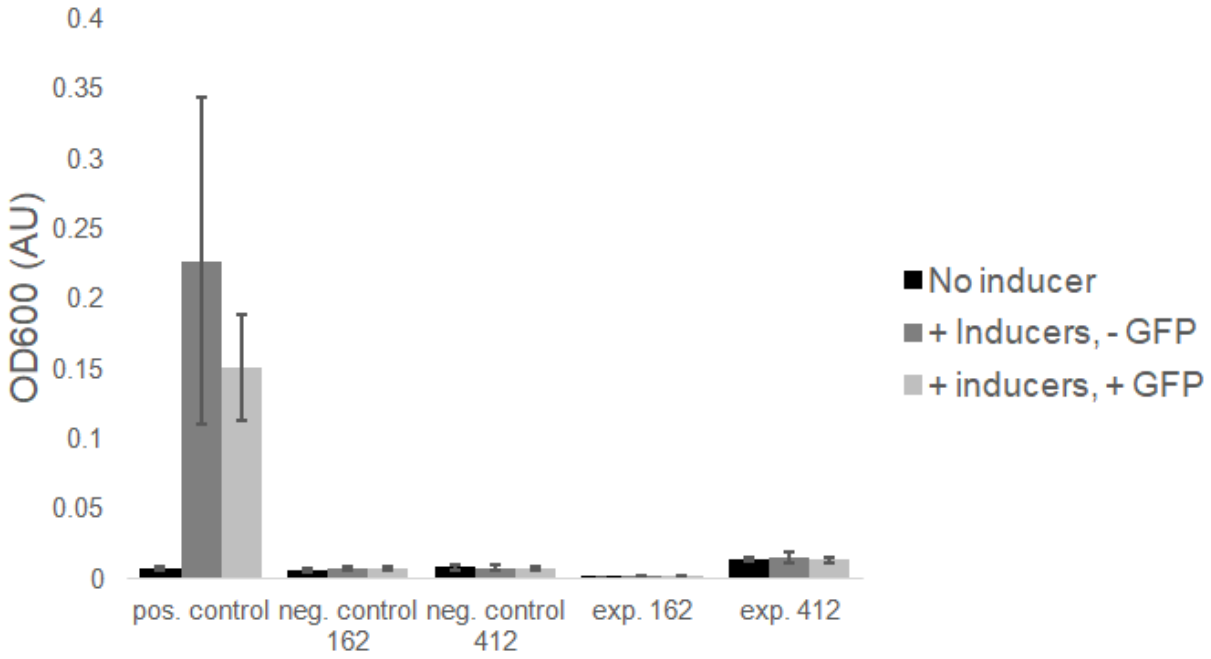

Figure 3.11. Current three-hybrid systems do not display protein-interaction-driven control of electron flow. When expression of ferredoxin-nanobody fusions and GFP is induced with 100 ng aTc (for Fd f1-LaG16/41), 100 μM IPTG (for Fd f2-LaG2) and 100 nM AHL (for GFP), no growth occurs in the sulfide auxotroph assay, showing that the presence of GFP is unable to cause ferredoxin complementation. Cells transformed with an unsplit ferredoxin and the AHL-induced GFP plasmid were used as a positive control. Cells transformed with the ferredoxin-nanobody fusions and an empty GFP vector were used as negative controls. The bars display the OD600 of cultures after 48 hours of growth in M9sa minimal media without sulfide. Error bars represent the standard deviation of three replicates.

Another strategy to couple free GFP expression to electron transfer uses the two-hybrid system. If free GFP were expressed alongside a Fd-nanobody and Fd-GFP fusion, then free GFP should compete with the Fd-GFP for the binding of the Fd-nanobody. Consequently, higher free

GFP expression should correlate with lower electron transfer activity exhibited by the two-hybrid system.

To test this strategy, the electron transfer activity of the construct 16_GFP was assessed at varying levels of GFP induction. When induction of the Fd-nanobody and Fd-GFP fusion expression was held constant and induction of free GFP expression was varied, electron transfer was inversely correlated with the level of GFP induction at early time points in the assay, which indicates that free GFP successfully competes with Fd-GFP for Fd-nanobody binding. However, at later time points the inverse correlation between GFP induction and electron transfer was abolished, as the highest GFP induction levels exhibited moderately high electron transfer activity (Figure 3.12a and b). Additionally, a control for this experiment—a strain transformed with the 16_GFP construct, the assay component vector, and an empty plasmid—behaved unexpectedly. This control strain is expected to show high growth no matter the level of GFP induction (as there is no GFP to induce expression of), but instead shows consistently low growth after 24 hrs incubation in selective assay conditions (Figure 3.12a). This means that this experiment should be repeated and that this strategy for linking GFP expression to electron transfer has not yet been demonstrated to function as expected.

(a)

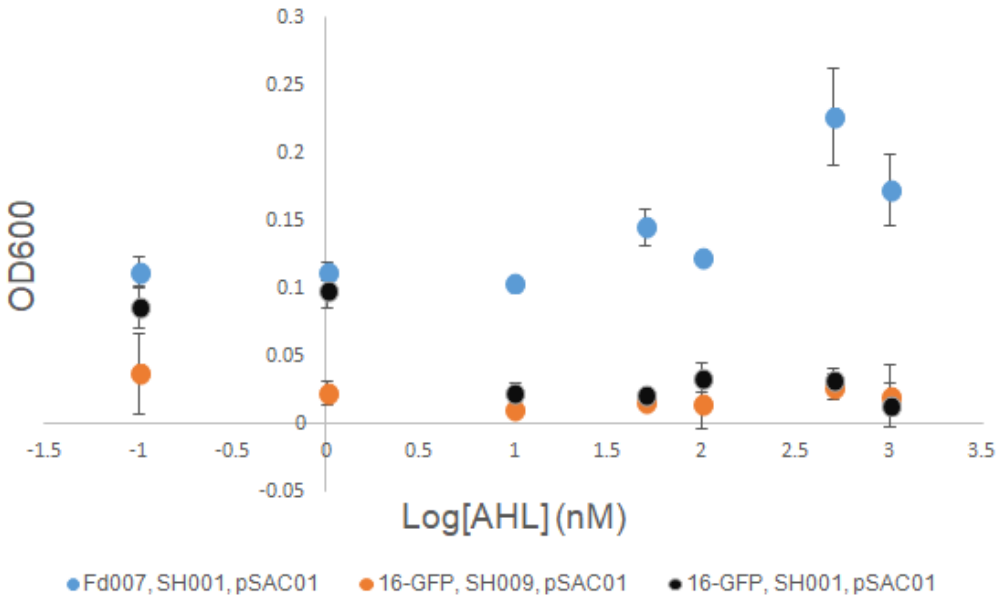

(b)

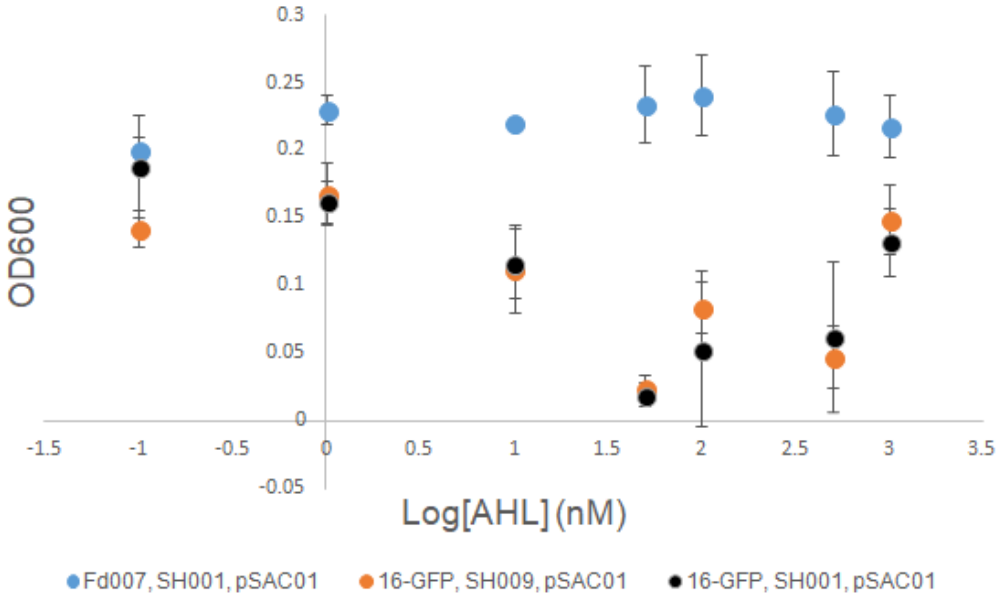

Figure 3.12. Free GFP may compete with Fd-GFP fusion for Fd-Nb fusion binding. (a) Electron transfer activity of 16_GFP construct is inversely correlated with free GFP induction after 24 hrs growth in sulfide auxotroph assay. When the expression of the 16_GFP construct components were induced with 100 ng/mL aTc and 100 µM IPTG, and free GFP (SH001) was induced using varying concentrations of AHL (0 nM, 0.1 nM, 1 nM, 10 nM, 50 nM, 100 nM, 500 nm, 1 µM), more growth in the sulfide auxotroph assay is seen at lower concentrations of AHL. In comparison, consistent growth in the sulfide auxotroph assay is seen when wild type *M. laminosus* Fd (Fd007) expression was induced with 100 ng/mL aTc and free GFP (SH001) was induced with varying concentrations of AHL. Consistent growth in the sulfide auxotroph assay is also seen when 16_GFP components were induced with 100 ng/mL aTc and 100 µM IPTG, and expression of an empty GFP vector (SH009) was induced with varying

concentrations of AHL. Markers represent the OD600 of cultures after 24 hrs growth in M9sa media. Error bars represent the standard deviation of three replicates. (b) The correlation between electron transfer activity and free GFP induction is lost at 48 hrs growth in sulfide auxotroph assay. Markers represent the OD600 of cultures after 48 hrs growth in M9sa media. Error bars represent the standard deviation of three replicates.

Both the three-hybrid system and free GFP competition with Fd-GFP have not yielded the expected results. Future work will include redesigning the three-hybrid system once more is known about the factors determining nanobody-driven Fd complementation are known, as well as repetition of the free GFP competition experiment.

3.5 Antibody domain insertion into ferredoxins

One final strategy for making electron transfer responsive to the presence of a free protein is to insert a nanobody into Fd, then mutate the nanobody so that it is unfolded in the absence of its target protein and folded in the presence of the target protein (Figure 3.2). When the target protein is present, the folded nanobody allows the Fd fragments on either side of the nanobody to complement and perform electron transfer, and when the target protein is absent, the unfolded nanobody prevents the Fd fragments from complementing and performing electron transfer.

To create this protein-dependent Fd, anti-GFP nanobodies (either Nb2, Nb16, or Nb41) were inserted after residue 35 of *M. laminosus* Fd. Flexible linkers with the sequence $(GGGGS)_2AAA$ were used to fuse the Fd fragments and nanobody. These domain-inserted Fds were put under the control of the inducible promoter P_{tet}. I first verified whether nanobody insertion affected the electron transfer activity of the Fd. Electron transfer activity was detected for Fds that contained a Nb2 or Nb16 domain, but not for the Fd containing a Nb41 domain at early time points in the Fd electron transfer assay (Figure 3.13a). However, at later time points,

the experimental controls started to behave unexpectedly, so these experiments should be repeated to confirm these early results (Figure 3.13b).

(a)

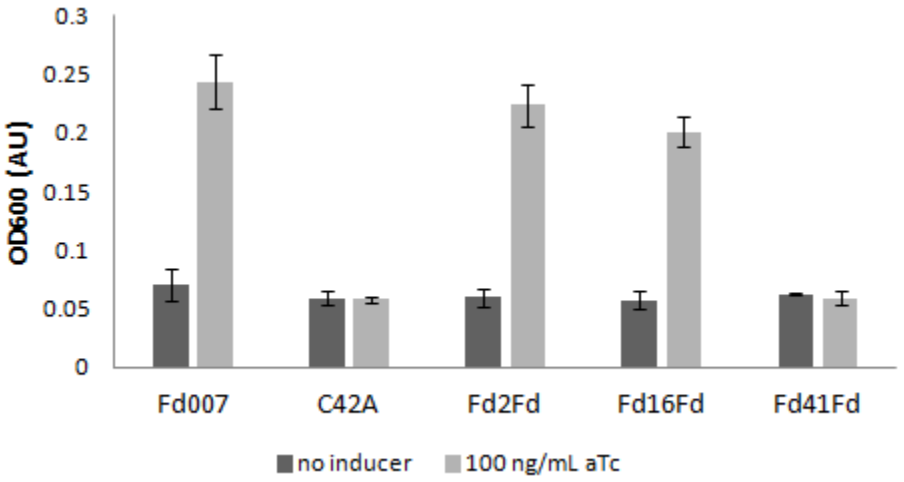

(b)

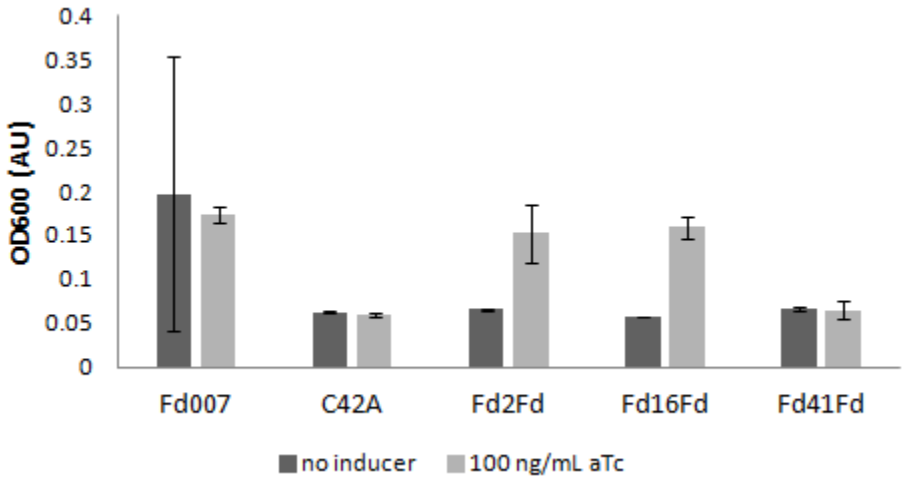

Figure 3.13. Ferredoxin may retain electron transfer after insertion of Nb2 or Nb16 after residue 35. (a) Nb2, Nb16, or Nb41 were inserted after residue 35 of Fd from *M. laminosus*, to create the constructs Fd2Fd, Fd16Fd, and Fd41Fd, respectively. When expression of the domain-inserted Fds from constructs Fd2Fd and Fd16Fd was induced with 100 ng/mL aTc, growth is seen in the sulfide auxotroph assay, indicating that insertion of Nb2 and Nb16 does not abolish the electron transfer activity of Fd. However, when expression of domain-inserted Fds from the construct Fd41Fd was induced using 100 ng/mL aTc, no growth is seen in the sulfide auxotroph assay, indicating that insertion of Nb41 somehow abolishes the electron transfer activity of Fd. The bars display the OD600 of cultures after 24 hours of growth in M9sa minimal media without sulfide. Error bars represent the standard deviation of three replicates. (b) After 48 hrs of incubation in M9sa minimal media without sulfide, cultures of sulfide auxotrophs transformed with a wild type Fd expression construct (Fd007) show growth even when no inducer is present, indicating problems with experimental conditions. These data indicate that these experiments may need to be repeated.

Further characterization of the domain insertion constructs is needed before mutation and screening of these nanobodies for conditional stability. The nanobodies' ability to bind GFP after insertion into Fd should be assessed. This can be done using a pull-down assay to test whether a domain-inserted Fd is pulled down with an affinity-tagged GFP.

Chapter 4: Future directions

4.1 Creating new electron transfer protein switches responsive to small molecules

Cytosolic protein switches engineered to transfer electrons only when specific small molecules are present may make useful biological sensors for molecules of interest. Such proteins can be expressed in microbes to turn them into living sensors which, when incorporated in bioelectronic devices, can be used to detect microbiome metabolites that are signatures of health and disease, environmental contaminants in various biomes, and other molecules whose concentrations are useful to measure. Because electron transfer is made dependent on a chemical-mediated change in protein conformation, the engineered protein switches can theoretically respond extremely rapidly (in seconds or less) to the presence of their chemical toggle. Fds have previously been made into protein switches for cytosolic regulation of ET, but these Fd-based switches have several drawbacks. First, the Fd switches that have been built are limited in their sensing repertoire. Current Fd switches respond to only two different molecules (rapamycin and 4-hydroxytamoxifen). Second, the Fd switches have not been fully characterized yet. The dynamic range of the switches—the electron transfer rate with and without the chemical toggle—is still unclear. Without this information, it is difficult to determine whether these switches will be sensitive enough to be useful in practical applications. Finally, because Fds use iron-sulfur cofactors to transfer electrons, expressing Fd switches may tie up iron in the cells that

is needed for other cell functions. This limits the utility of these switches in microbiomes in which there is little total iron, such as the ocean, or in environments where iron is inaccessible to the engineered cells, such as the human gut, where there are microbes like pseudomonads that use siderophores to scavenge free iron from the environment, and soils with high pH, in which iron is poorly soluble. Because iron availability can vary across microbiomes where electrical biosensing may be desired, it would be beneficial to create switches that use an organic cofactor to mediate ET (Rijkenberg et al, 2014, Gotoh, S., & Patrick, W. H.,1974).

Flavodoxins are electron transfer proteins that use a flavin mononucleotide cofactor to perform electron transfer and are possible targets for new switches. Flds often substitute for Fds in species that live in iron-deficient environments, and we have data to show that Flds can transfer electrons to and from partners that natively transfer electrons to and from Fds, and that Fld electron transfer can be selected in a protein design experiment using a strategy identical to that achieved with Fds (Campbell et al, 2019). This suggests that the approaches (such as insertion of estrogen receptor ligand binding domain) that were used to create Fd switches can applied to Flds to create Fld switches that can function in iron-limited environments. There are several constraints on the design of these switches. First, the specific Fld that is the basis of these switches should be thermostable enough to tolerate domain insertion. Second, the Fld should be compatible in the cellular assay used to evaluate Fd switches. Finally, since Flds are cytosolic proteins, the ligand that it senses should be able to pass through the bacterial cell wall into the cytosol. This means that possible ligand candidates should be <500 Da, as this is the maximum size molecule that bacterial porins allow entry into the cell (Nikaido, 1994). I hypothesize that chemical-dependent Fld switches that are toggled by signatures of gut health can be created by inserting the estrogen binding domain or other ligand binding domains into a Fld (Table 6). A

cellular selection can mine libraries for switch functions that are desired, and the substrate specificity of the switches can be tuned by mutating the ligand binding site so that they support cell growth in the presence of ligands listed in Table 4.1.

Table 4.1. Possible target analytes and the diseases associated with them.
(1) Le Gall et al, 2011 (2) Antharam et al, 2016. (3) Theriot et al, 2014 (4) Heinken et al, 2019 (5) Duboc et al, 2013 (6) Yachida et al, 2019

Analyte	**MW (Da)**	**Gut address**	**Disease**	**Impact on homeostasis**
Taurine[1]	125.2	Colon	Ulcerative Colitis and IBS	Increased
Cadaverine[1]	101.2	Colon	Ulcerative Colitis	Increased
Choline[1]	104.2	Colon	UC + IBS	Increased
Glucose[1]	180.2	Colon	UC + IBS	Increased
2-methylbutyrate[1]	116.2	Colon	UC + IBS	Increased
Isovalerate[1]	101.1	Colon	IBS	Lowered
Cholesterol[2]	386.7	Colon	C. diff	Increased
Coprostanol[2]	388.7	Colon	C. diff	Decreased
Primary Bile acids		Secreted into duodenum and reabsorbed in ileum, ~5% passes into colon		
Cholic acid (CA)	408.6			
Chenodeoxycholic acid (CDCA)	392.6			
Taurocholic acid (Tauro-CA)[3]	515.7		Associated w/ C. diff susceptibility	Increased (8.02 ug/mg) after antibiotic treatment
Glycocholic acid (Glyco-CA)	465.6			
Taurochenodeoxycholate (Tauro-CDCA)	579.8			
Glycochenodeoxycholate (Glyco-CDCA)	449.6			
Secondary bile acids[4, 5]			Inflammatory bowel disease, colon cancer	Decreased (IBD), Increased (cancer)
12-dehydrocholate (12-dehydro-CA)	424.5			
7-ketodeoxycholate (7-keto-CA)	406.6			
7-dehydrochenodeoxycholate (7-dehydro-CDCA)	389.5			
3-dehydrocholate (3-dehydro-CA)	406.6			
3-dehydrochenodeoxycholate (3-dehydro-CDCA)	389.5			
Isocholate (Iso-CA)	407.6			
Isochenodeoxycholate (Iso-CDCA)	391.6			
Lithocholate (LCA)	376.6			

Deoxycholic acid (DCA)[6]	392.6		IBS + multiple polypoid adenomas/intramucosal carcinomas	Increased
Allolithocholate (allo-LCA)	376.6			
Allodeoxycholate (allo-DCA)	392.6			
Ursocholate (UCA)	408.6			
Ursodeoxycholic acid (UDCA)	392.6			

4.2 Experimental plan

1. Create a library of split flavodoxins using pooled oligo synthesis.

2. Clone the synthesized genes into a plasmid to create a naïve library.

3. Clone the ER binding domain/other ligand binding domains into split flavodoxin library.

4. Transform libraries into cells and use cellular selection to select for sequences that show desired behavior in the presence and absence of the analyte.

5. Deep sequence the naïve library and selected library.

6. Analyze deep sequencing data to identify which sequences are significantly enriched when analyte is present compared to naïve and no-ligand conditions.

7. Validate and characterize switches in cellular assay.

8. Plug switches into pathway that connects with Mtr, a cell membrane complex that allows extracellular electron transfer.

4.3 Creating new electron transfer protein switches responsive to macromolecules

There are a limited number of ligand binding domains that have the desired ligand-dependent conformational change, restricting the number of possible chemicals that the switch can report on. The ER ligand binding domain provides a platform for engineering sensing of

estrogen-like molecules (steroids) but is less suited to binding other small molecules. We could expand the repertoire of molecules that ER LBD binds to by mutating it to have stronger binding affinity for other molecules. However, it is unlikely that ER LBD can be mutated to have affinity for completely new classes of molecules. Instead of hunting for a specific native binding domain with the desired ligand-dependent conformational change for each class of molecule that we want to sense, or altering ER LBD to bind new ligands of interest, it might be possible to take a protein that binds our molecule of interest and mutate it to display ligand-dependent conformational change. One class of binding proteins, nanobodies, which are small, single-domain antibody derivatives, are well-suited to expression in bacteria. I hypothesize that nanobodies engineered to be stable only in the presence of their binding target can be inserted into Fd/Flds to introduce allosteric control to them.

4.4 Experimental plan

1. Insert anti-GFP nanobodies into Fds as initial test bed (continuation of BA/MA work).
2. Screen for variants that function +/- GFP expression.
3. Of the functioning variants, rescreen for variants that show significantly different Fd activity between +GFP and -GFP conditions.
    a. likely logic: -GFP → active Fd; +GFP → inactive Fd (GFP is likely to block Fd/Fld partner binding)
4. If no variant with GFP-dependent activity is found, mutate nanobody, and rescreen.
    b. alternate logic: -GFP → inactive Fd; +GFP → active Fd (Fd-Nb fusion destabilized so that it is not functional until you gain free energy from binding Nb ligand)
5. Insert Nb into discovered split Flds and repeat 2-4 for Fld variants.

References

Antharam, V.C., McEwen, D.C., Garrett, T.J., Dossey, A.T., Li, E.C., Kozlov, A.N., Mesbah, Z., and Wang, G.P. (2016). An Integrated Metabolomic and Microbiome Analysis Identified Specific Gut Microbiota Associated with Fecal Cholesterol and Coprostanol in Clostridium difficile Infection. PLOS ONE *11*, e0148824.

Atkinson, J.T., Campbell, I.J., Thomas, E.E., Bonitatibus, S.C., Elliott, S.J., Bennett, G.N., and Silberg, J.J. (2019). Metalloprotein switches that display chemical-dependent electron transfer in cells. Nature Chemical Biology *15*, 189.

Atkinson, J.T., Campbell, I.J., Thomas, E.E., Bonitatibus, S.C., Elliott, S.J., Bennett, G.N., and Silberg, J.J. (2019). Metalloprotein switches that display chemical-dependent electron transfer in cells. Nature Chemical Biology *15*, 189.

Barstow, B., Agapakis, C.M., Boyle, P.M., Grandl, G., Silver, P.A., and Wintermute, E.H. (2011). A synthetic system links FeFe-hydrogenases to essential E. coli sulfur metabolism. Journal of Biological Engineering *5*, 7.

Battistuzzi, G., D'Onofrio, M., Borsari, M., Sola, M., Macedo, A. L., Moura, J. J., and Rodrigues, P. (2000) Redox thermodynamics of low-potential iron-sulfur proteins. JBIC, J. Biol. Inorg. Chem. 5, 748− 760.

Bird, R.E., Hardman, K.D., Jacobson, J.W., Johnson, S., Kaufman, B.M., Lee, S.M., Lee, T., Pope, S.H., Riordan, G.S., and Whitlow, M. (1988). Single-chain antigen-binding proteins. Science *242*, 423–426.

Black, W.B., Zhang, L., Mak, W.S., Maxel, S., Cui, Y., King, E., Fong, B., Sanchez Martinez, A., Siegel, J.B., and Li, H. (2020). Engineering a nicotinamide mononucleotide redox cofactor system for biocatalysis. Nature Chemical Biology *16*, 87–94.

Calzadiaz-Ramirez, L., Calvó-Tusell, C., Stoffel, G.M.M., Lindner, S.N., Osuna, S., Erb, T.J., Garcia-Borràs, M., Bar-Even, A., and Acevedo-Rocha, C.G. (2020). In Vivo Selection for Formate Dehydrogenases with High Efficiency and Specificity toward NADP+. ACS Catal. *10*, 7512–7525.

Campbell, I.J., Bennet, G.N., and Silberg, J.J. (2019). Evolutionary Relationships Between Low Potential Ferredoxin and Flavodoxin Electron Carriers | Energy Research. Front. Energy Res. *7*, 1–18.

Dammeyer, T., Bagby, S.C., Sullivan, M.B., Chisholm, S.W., and Frankenberg-Dinkel, N. (2008). Efficient Phage-Mediated Pigment Biosynthesis in Oceanic Cyanobacteria. Current Biology *18*, 442–448.

Duboc, H., Rajca, S., Rainteau, D., Benarous, D., Maubert, M.-A., Quervain, E., Thomas, G., Barbu, V., Humbert, L., Despras, G., et al. (2013). Connecting dysbiosis, bile-acid dysmetabolism and gut inflammation in inflammatory bowel diseases. Gut *62*, 531–539.

Fish, A., Danieli, T., Ohad, I., Nechushtai, R., and Livnah, O. (2005). Structural Basis for the Thermostability of Ferredoxin from the Cyanobacterium Mastigocladus laminosus. Journal of Molecular Biology *350*, 599–608.

Fridy, P.C., Li, Y., Keegan, S., Thompson, M.K., Nudelman, I., Scheid, J.F., Oeffinger, M., Nussenzweig, M.C., Fenyö, D., Chait, B.T., et al. (2014). A robust pipeline for rapid production of versatile nanobody repertoires. Nature Methods *11*, 1253–1260.

Gotoh, S., & Patrick, W. H. (1974). Transformation of iron in a waterlogged soil as influenced by redox potential and pH 1. *Soil Science Society of America Journal*, **38**, 66– 71.

Harmsen, M.M., and De Haard, H.J. (2007). Properties, production, and applications of camelid single-domain antibody fragments. Appl Microbiol Biotechnol *77*, 13–22.

Heinken, A., Ravcheev, D.A., Baldini, F., Heirendt, L., Fleming, R.M.T., and Thiele, I. (2019). Systematic assessment of secondary bile acid metabolism in gut microbes reveals distinct metabolic capabilities in inflammatory bowel disease. Microbiome *7*, 75.

Hill, Z.B., Martinko, A.J., Nguyen, D.P., and Wells, J.A. (2018). Human antibody-based chemically induced dimerizers for cell therapeutic applications. Nat. Chem. Biol. *14*, 112–117.

Jang, J.K., Pham, T.H., Chang, I.S., Kang, K.H., Moon, H., Cho, K.S., and Kim, B.H. (2004). Construction and operation of a novel mediator- and membrane-less microbial fuel cell. Process Biochemistry *39*, 1007–1012.

Kim, B.H., Chang, I.S., and Gadd, G.M. (2007). Challenges in microbial fuel cell development and operation. Appl Microbiol Biotechnol *76*, 485–494.

Kochanowski, K., Sauer, U., and Noor, E. (2015). Posttranslational regulation of microbial metabolism. Current Opinion in Microbiology *27*, 10–17.

Le Gall, G., Noor, S.O., Ridgway, K., Scovell, L., Jamieson, C., Johnson, I.T., Colquhoun, I.J., Kemsley, E.K., and Narbad, A. (2011). Metabolomics of Fecal Extracts Detects Altered Metabolic Activity of Gut Microbiota in Ulcerative Colitis and Irritable Bowel Syndrome. J. Proteome Res. *10*, 4208–4218.

Li, G., Zhu, M., Ma, L., Yan, J., Lu, X., Shen, Y., and Wan, Y. (2016). Generation of Small Single Domain Nanobody Binders for Sensitive Detection of Testosterone by Electrochemical Impedance Spectroscopy. ACS Appl. Mater. Interfaces *8*, 13830–13839.

Logan, B.E. (2009). Exoelectrogenic bacteria that power microbial fuel cells. Nature Reviews Microbiology *7*, 375–381.

Logan, B.E., Hamelers, B., Rozendal, R., Schröder, U., Keller, J., Freguia, S., Aelterman, P., Verstraete, W., and Rabaey, K. (2006). Microbial Fuel Cells: Methodology and Technology †. Environ. Sci. Technol. *40*, 5181–5192.

Lovley, D.R. (2011). Powering microbes with electricity: direct electron transfer from electrodes to microbes. Environmental Microbiology Reports *3*, 27–35.

McMahon, C., Baier, A.S., Pascolutti, R., Wegrecki, M., Zheng, S., Ong, J.X., Erlandson, S.C., Hilger, D., Rasmussen, S.G.F., Ring, A.M., et al. (2018). Yeast surface display platform for rapid discovery of conformationally selective nanobodies. Nature Structural & Molecular Biology *25*, 289–296.

Mellor, S.B., Nielsen, A.Z., Burow, M., Motawia, M.S., Jakubauskas, D., Møller, B.L., and Jensen, P.E. (2016). Fusion of Ferredoxin and Cytochrome P450 Enables Direct Light-Driven Biosynthesis. ACS Chem Biol *11*, 1862–1869.

Mimee, M., Nadeau, P., Hayward, A., Carim, S., Flanagan, S., Jerger, L., Collins, J., McDonnell, S., Swartwout, R., Citorik, R.J., et al. (2018). An ingestible bacterial-electronic system to monitor gastrointestinal health. Science *360*, 915–918.

Monk, J.M., Lloyd, C.J., Brunk, E., Mih, N., Sastry, A., King, Z., Takeuchi, R., Nomura, W., Zhang, Z., Mori, H., et al. (2017). iML1515, a knowledgebase that computes Escherichia coli traits. Nature Biotechnology *35*, 904–908.

Nelson, D.L., and Cox, M.M. (2017). Chapter 14 Glycolysis, Gluconeogenesis, and the Pentose Phosphate Pathway. In Lehninger Principles of Biochemistry, (W. H. Freeman and Company), pp. 533–574.

Nelson, D.L., and Cox, M.M. (2017). Chapter 16 The Citric Acid Cycle. In Lehninger Principles of Biochemistry, (W. H. Freeman and Company), pp. 619–647.

Nelson, D.L., and Cox, M.M. (2017). Chapter 20 Photosynthesis and Carbohydrate Synthesis in Plants. In Lehninger Principles of Biochemistry, (W. H. Freeman and Company), pp. 755–810.

Nevin, K.P., Hensley, S.A., Franks, A.E., Summers, Z.M., Ou, J., Woodard, T.L., Snoeyenbos-West, O.L., and Lovley, D.R. (2011). Electrosynthesis of Organic Compounds from Carbon Dioxide Is Catalyzed by a Diversity of Acetogenic Microorganisms. Appl. Environ. Microbiol. *77*, 2882–2886.

Nikaido, H. (1994). Porins and Specific Diffusion Channels in Bacterial Outer Membranes. J. Biol. Chem. *269*, 3905–3908.

Pardon, E., Laeremans, T., Triest, S., Rasmussen, S.G.F., Wohlkönig, A., Ruf, A., Muyldermans, S., Hol, W.G.J., Kobilka, B.K., and Steyaert, J. (2014). A general protocol for the generation of Nanobodies for structural biology. Nat Protoc *9*, 674–693.

Prévoteau, A., Carvajal-Arroyo, J.M., Ganigué, R., and Rabaey, K. (2020). Microbial electrosynthesis from CO2: forever a promise? Current Opinion in Biotechnology *62*, 48–57.

Reeve, J. N., Beckler, G. S., Cram, D. S., Hamilton, P. T., Brown, J. W., Krzycki, J. A., Kolodziej, A. F., Alex, L., Orme-Johnson, W. H., and Walsh, C. T. (1989) A hydrogenase-linked gene in Methanobacterium thermoautotrophicum strain delta H encodes a polyferredoxin. Proc. Natl. Acad. Sci. U. S. A. 86, 3031−3035.

Rijkenberg, M.J.A., Middag, R., Laan, P., Gerringa, L.J.A., Aken, H.M. van, Schoemann, V., Jong, J.T.M. de, and Baar, H.J.W. de (2014). The Distribution of Dissolved Iron in the West Atlantic Ocean. PLOS ONE *9*, e101323.

Shen, C.R., Lan, E.I., Dekishima, Y., Baez, A., Cho, K.M., and Liao, J.C. (2011). Driving Forces Enable High-Titer Anaerobic 1-Butanol Synthesis in Escherichia coli. Appl. Environ. Microbiol. *77*, 2905–2915.

Shi, L., Dong, H., Reguera, G., Beyenal, H., Lu, A., Liu, J., Yu, H.-Q., and Fredrickson, J.K. (2016). Extracellular electron transfer mechanisms between microorganisms and minerals. Nat. Rev. Microbiol. *14*, 651–662.

Spinelli, S., Frenken, L., Bourgeois, D., Ron, L. de, Bos, W., Verrips, T., Anguille, C., Cambillau, C., and Tegonil, M. (1996). The crystal structure of a llama heavy chain variable domain. Nature Structural Biology *3*, 752.

Spinelli, S., Tegoni, M., Frenken, L., van Vliet, C., and Cambillau, C. (2001). Lateral recognition of a dye hapten by a llama VHH domain11Edited by I. Wilson. Journal of Molecular Biology *311*, 123–129.

TerAvest, M.A., Zajdel, T.J., and Ajo-Franklin, C.M. (2014). The Mtr Pathway of Shewanella oneidensis MR-1 Couples Substrate Utilization to Current Production in Escherichia coli. ChemElectroChem *1*, 1874–1879.

Theriot, C.M., Koenigsknecht, M.J., Carlson, P.E., Hatton, G.E., Nelson, A.M., Li, B., Huffnagle, G.B., Z. Li, J., and Young, V.B. (2014). Antibiotic-induced shifts in the mouse gut microbiome and metabolome increase susceptibility to Clostridium difficile infection. Nature Communications *5*, 3114.

Thompson, L.R., Zeng, Q., Kelly, L., Huang, K.H., Singer, A.U., Stubbe, J., and Chisholm, S.W. (2011). Phage auxiliary metabolic genes and the redirection of cyanobacterial host carbon metabolism. Proc Natl Acad Sci U S A *108*, E757–E764.

Voß, S., Klewer, L., and Wu, Y.-W. (2015). Chemically induced dimerization: reversible and spatiotemporal control of protein function in cells. Current Opinion in Chemical Biology *28*, 194–201.

Wang, M., Chen, B., Fang, Y., and Tan, T. (2017). Cofactor engineering for more efficient production of chemicals and biofuels. Biotechnology Advances *35*, 1032–1039.

Webster, D.P., TerAvest, M.A., Doud, D.F.R., Chakravorty, A., Holmes, E.C., Radens, C.M., Sureka, S., Gralnick, J.A., and Angenent, L.T. (2014). An arsenic-specific biosensor with

genetically engineered Shewanella oneidensis in a bioelectrochemical system. Biosens Bioelectron *62*, 320–324.

Wu, B., Atkinson, J.T., Kahanda, D., Bennett, G.N., and Silberg, J.J. (2020). Combinatorial design of chemical-dependent protein switches for controlling intracellular electron transfer. AIChE Journal *66*, e16796.

Yachida, S., Mizutani, S., Shiroma, H., Shiba, S., Nakajima, T., Sakamoto, T., Watanabe, H., Masuda, K., Nishimoto, Y., Kubo, M., et al. (2019). Metagenomic and metabolomic analyses reveal distinct stage-specific phenotypes of the gut microbiota in colorectal cancer. Nature Medicine *25*, 968–976.

Yacoby, I., Pochekailov, S., Toporik, H., Ghirardi, M. L., King, P. W., and Zhang, S. (2011) Photosynthetic electron partitioning between [FeFe]-hydrogenase and ferredoxin:NADP+-oxidoreductase (FNR) enzymes in vitro. Proc. Natl. Acad. Sci. U. S. A. 108, 9396−9401.

Yacoby, I., Pochekailov, S., Toporik, H., Ghirardi, M.L., King, P.W., and Zhang, S. (2011). Photosynthetic electron partitioning between [FeFe]-hydrogenase and ferredoxin:NADP+-oxidoreductase (FNR) enzymes in vitro. PNAS *108*, 9396–9401.

Yan, J., Li, G., Hu, Y., Ou, W., and Wan, Y. (2014). Construction of a synthetic phage-displayed Nanobody library with CDR3 regions randomized by trinucleotide cassettes for diagnostic applications. J Transl Med *12*, 343.